Geological Magazine

www.cambridge.org/geo

Original Article

Cite this article: Basumatary P, Saikia A, Prakash T, and Gogoi B (2023) Geochemical constraints on the petrogenesis of mafic rocks (metadolerites) from the Proterozoic Shillong Basin, Northeast India: implications for growth of the Greater Indian Landmass. *Geological Magazine* **160**: 1114–1130. https://doi.org/10.1017/S0016756823000237

Received: 23 August 2022
Revised: 17 March 2023
Accepted: 27 March 2023
First published online: 27 April 2023

Keywords:
Subduction-related magmatism; Back-arc basalt; Amphibolite facies metamorphism; Mikir Massif; Central Indian Tectonic Zone

Corresponding author:
Bibhuti Gogoi,
Email: bibhuti.gogoi.baruah@gmail.com

Geochemical constraints on the petrogenesis of mafic rocks (metadolerites) from the Proterozoic Shillong Basin, Northeast India: implications for growth of the Greater Indian Landmass

Pallabi Basumatary[1], Ashima Saikia[2], Tribujjal Prakash[1] and Bibhuti Gogoi[1]

[1]Department of Geology, Cotton University, Guwahati, Assam, India and [2]Department of Geology, University of Delhi, Delhi, India

Abstract

The Paleo-Mesoproterozoic Shillong Basin of the Assam-Meghalaya Gneissic Complex is exposed in parts of Northeast India. The studied metadolerites are from the volcano-sedimentary sequence of Shillong Basin from the Borjuri area in the Mikir Massif. This episode of mafic magmatism can be correlated with the Columbia supercontinent formation and bears significance to its reconstruction. The present work discusses the field, petrography and geochemical characteristics of the metadolerites, which occur in close association with the quartzites of the Shillong Group of rocks (metasedimentary rocks of the Shillong Basin). Our data show distinctive characteristics of subduction-related magmatism exhibiting high LREE/HREE, large ion lithophile element/high field strength element ratios and pronounced negative Nb anomaly. Elemental ratios such as Zr/Ba (0.21–0.46), La/Nb (1.23–2.32) and Ba/Nb (30.08–56.90) point to a fluid-enriched lithospheric mantle source in a subduction regime. Metadolerites plot in the field of 'back-arc basin basalts' in tectonic discrimination diagrams reinforcing a subduction zone tectonic setting. The mafic rocks correspond to a 6–10 % partial melting of a mantle source incorporating spinel+garnet lherzolite. The metamorphic P-T of the metadolerites estimated from plagioclase-hornblende geothermobarometer (7–8 kbar, 664 °C) is indicative of amphibolite facies metamorphism in a medium P-T zone. Based on the comparative analysis of field observation, petrography, geochemistry and geological ages given by previous workers, we infer that the Shillong Basin represents a back-arc rift region and is the eastern continuation of the Bathani volcano-sedimentary sequence of the Chotanagpur Granite Gneiss Complex marking continuation of the Central Indian Tectonic Zone to the Mikir Massif.

1. Introduction

The genesis of mafic magma in both interplate and intraplate areas is a key concern in igneous petrology. Mafic magmas are generated as a result of (i) rise of local geothermal gradient by physical convection, (ii) subsequent lowering of solidus by influx of volatile constituents or by (iii) localized spike in geothermal gradient (frictional heating) due to tectonic conditions (Wyllie, 1988). Mafic magmas also undergo fractional crystallization and crustal contamination, which facilitates change in their chemical composition (Rollinson, 1993; Pe-piper *et al.* 2003). Variations in the trace element and isotopic abundances in the mafic magmas point to geochemically distinct sources in the mantle (Wyllie, 1988). The presence or absence of incompatible/mobile trace elements and high/low isotopic signatures in the melt can define a source as enriched or depleted (Pearce & Norry, 1979; Anderson, 1995). Melts from the depleted reservoir are mostly prominent at spreading ridges. On the other hand, it is suggested that enriched magmas are most evident in infant subduction zones, new rifting regions and intraplate environments away from spreading ridges (Anderson, 1995). Therefore, geochemical studies of mafic igneous rocks can provide insights into the processes of generation of mafic magmas from mantle, magma evolution and related tectonic setting.

The Indian subcontinent is endowed with mafic magmatic bodies emplaced over a wide range of time intervals from the Archaean belts of south India to the Cretaceous-Tertiary Deccan basalt sequences (Watts & Cox, 1989; Ahmad & Tarney, 1991). Imprints of mafic magmatism are observed in all the Precambrian cratonic blocks of the Indian shield (Ray *et al.* 2013). Numerous mobile belts separate these cratonic blocks. Among the prominent mobile belts, the Central Indian Tectonic Zone (CITZ) is an E-W striking belt, extending eastward through the Chotanagpur Granite Gneiss Complex (CGGC) to the Assam-Meghalaya Gneissic Complex (AMGC) (Acharyya, 2001). The AMGC of northeastern India comprises

a variety of rock types including migmatitic gneisses, metasedimentary rocks, mafic magmatic rocks and several granitoid plutons. It is considered that thermal disturbances in the upper mantle initiated rifting within the AMGC resulting in the formation of a basin now known as the Shillong Basin. Subsequent sedimentation within this basin resulted in the formation of the Shillong Group of metasedimentary rocks (Bhattacharjee & Rahman, 1985). A group of mafic intrusives (i.e. metadolerites) are found within the Shillong Group of rocks. These intrusives are considered evidence of subduction-related mafic magmatism in the AMGC (Ray *et al.* 2013). Stratigraphically, they have been classified as the Khasi greenstones (Mazumder, 1986; Srinivasan *et al.* 1996).

Studies on mafic rocks from different parts of the CITZ have been carried out by various researchers (Ghosh *et al.* 2005; Kumar & Ahmad, 2007; Ghose & Chatterjee, 2008; Srivastava & Ahmad, 2008; Ahmad & Wanjari, 2009; Srivastava, 2012; Alam *et al.* 2017; Ahmad *et al.* 2021). However, work on its easternmost extension, that is, the AMGC, is limited. Even though some amount of work has been done on the Proterozoic mafic rocks (i.e. Khasi greenstone) of the Khasi Hills in Meghalaya (Hazra & Ray, 2009; Mallikharjuna *et al.* 2009; Ray *et al.* 2013), very few reports exist on the mafic rocks of the Mikir Massif in Assam. This paper focuses on the Proterozoic mafic rocks (metadolerites) of the Mikir Massif. Petrological studies on the basis of field relationships, petrography, mineral compositional analyses with electron probe micro-analyser and geochemistry with major and trace element data are being carried out to give a detailed overview of the genesis of these rocks and their tectonic setting. Inferences of the study will elucidate the formation of the Proterozoic Shillong Basin.

2. Geological setting

The CITZ is an ENE–WSW-trending Proterozoic mobile belt which divides the Greater Indian Landmass into two crustal provinces, viz. Northern Indian Block and Southern Indian Block (Acharyya, 2003). The Mahakoshal Mobile Belt (MMB) occupies the northern region of the CITZ, while the southern belt of the CITZ consists of the Sausar Mobile Belt, the CGGC and the AMGC. The Bathani volcano-sedimentary sequence (BVSs) is a volcano-sedimentary suite located in the northern fringe of the CGGC and is the eastern continuation of the MMB. Bora *et al.* (2013) attained a U–Pb SHRIMP zircon $^{206}Pb/^{238}U$ age of 1753 ± 9 Ma, and Yadav *et al.* (2015) reported a U–Pb ID-TIMS zircon age of 1873 ± 13 Ma from the calc-alkaline granitoids of MMB. Chatterjee & Ghose (2011) obtained a 1697±17 Ma monazite crystallization age from the porphyritic granites of northern CGGC close to BVSs. Saikia *et al.* (2017, 2019) reported a U–Pb ID-TIMS ages of ca. 1700–1600 Ma and a Rb-Sr whole rock isochron age of 1664 ± 130 Ma for the granites of BVSs.

The AMGC is the lone illustration of the Proterozoic gneissic basement rocks in Northeast India. This area is tectonically disconnected from mainland India by the Garo-Rajmahal depression (Eremenco *et al.* 1969). The AMGC is also flanked by two subduction zones, viz. (i) the Indian Plate subducted beneath the Burmese Plate to its southeast and (ii) Indian Plate subducted beneath the Eurasian Plate to its north. This seismically and geodynamically active area is suggested to be the eastern extension of the Chotanagpur Granite Gneissic Complex (Desikachar, 1974). This sector is restricted dominantly in the states of Meghalaya and Assam in Northeast India. The Mikir Massif is separated from the Meghalaya part of AMGC by the NW-SE-trending Kopili lineament (Fig. 1). The NE-SW-trending Mesoproterozoic Shillong Basin occupies the northwestern part of Mikir Massif.

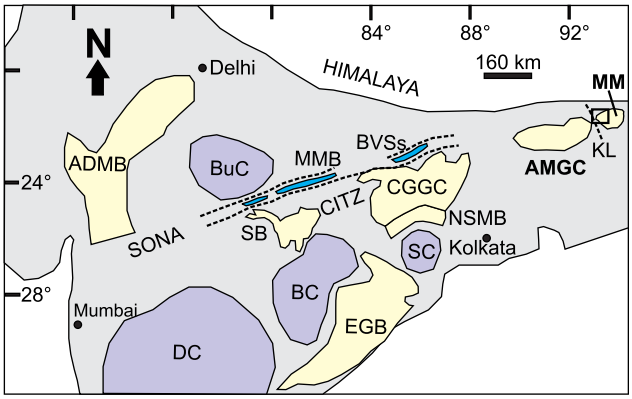

Figure 1. (Colour online) Tectonic map of India showing the location of Mikir Massif (MM) along with the Archean cratons and Proterozoic mobile belts (modified after Chatterjee & Ghose, 2011). The study area is shown within the black square. Abbreviations: ADMB, Aravalli Delhi Mobile Belt; AMGC, Assam-Meghalaya Gneissic Complex; BC, Bastar Craton; BuC, Bundelkhand Craton; BVSs, Bathani volcano-sedimentary sequence; CGGC, Chotanagpur Granite Gneiss Complex; CITZ, Central Indian Tectonic Zone; DC, Dharwar Craton; EGB, Eastern Ghats Belt; KL, Kopili Lineament; MMB, Mahakoshal Mobile Belt, MM, Mikir Massif; NSMB: North Singhbhum Mobile Belt; SB, Satpura Belt; SC, Singhbhum Craton; SONA, Son-Narmada lineaments.

Lithologically, the AMGC comprises basement gneissic complex, amphibolites, migmatites, calc-silicate rocks, granulites, Shillong Group of metasedimentary rocks and Mesozoic-Tertiary igneous and sedimentary rocks (Nandy, 2001; Srivastava & Sinha, 2004). The Shillong Group of rocks is divided into two formations, viz. the Lower Metapelitic Formation and the Upper Quartzitic Formation. The Shillong Group of rocks unconformably overlies the basement gneissic complex (Nandy, 2001; Srivastava & Sinha, 2004). Several discordant granitoid plutons (500–700 Ma) are found intruded within the basement gneissic complex as well as the Shillong Group of rocks (Ghosh *et al.* 1991; Kumar, 1990). Moreover, Gogoi *et al.* (2019) reported an LA-inductively coupled plasma mass spectrometry (ICP-MS) U–Pb zircon age of 1644 ± 33 Ma, 1599 ± 17 Ma and 1550 ± 25 Ma from the porphyritic granites of Shillong Basin in the Mikir Massif. Metadolerites occur as concordant and discordant bodies within the Shillong Group (Fig. 2) and are referred to as Khasi greenstone (Mazumder, 1986). These Khasi greenstones had been subjected to low-grade metamorphism (Srinivasan *et al.* 1996).

The major lithological components of the Mikir Massif consist of amphibolites, sillimanite-bearing gneisses, granulites, banded iron formation and granite gneisses (Ghosh *et al.* 2005; Gogoi *et al.* 2019). The Shillong Group of rocks in Mikir Massif is illustrated by low-grade schists such as quartz sericite, garnetiferous and ferruginous schists, quartzite, conglomerate and cross-bedded arenites (Dhurandhar *et al.* 2019), although the Mikir Massif is similar in lithology to the Meghalaya part of AMGC but it differs in the metamorphic grade. A generalized stratigraphic succession of the Mikir Massif is presented in Table 1. The present study is carried out near the Borjuri village of Assam in Northeast India. Here, metadolerites related to the Khasi greenstone are found to be in contact with quartzites of the Shillong Group. These mafic bodies are exposed at a number of places within the Shillong Group of rocks. However, due to very thick vegetation, it is difficult to undertake field investigations in our study area. The present

https://doi.org/10.1017/S0016756823000237 Published online by Cambridge University Press

Table 1. A generalized stratigraphic succession of Mikir Massif (after Awati *et al.* 1995; Majumdar & Gogoi, 2020)

Geological age	Group	Formation	Lithology
Tertiary			Thin bedded low dipping friable sandstone
~ ~ ~ ~ ~ ~ ~ ~ ~ ~ ~ ~	~Unconformity	~ ~ ~ ~ ~ ~ ~ ~ ~ ~	~ ~ ~ ~ ~ ~ ~ ~ ~ ~ ~ ~
Cretaceous (83 ± 13 to 90 ± 10 Ma) (105–117 Ma)			Carbonatite complex, mafic dykes, sills and traps
Cambro-Ordovician (518–470 Ma)		Non-porphyritic granitoids	Medium fine grained
Mesoproterozoic (1100–1000 Ma) (1644–1550 Ma)		Porphyritic granitoids	Fine-grained porphyry granite, light to dark grey, pink, coarse-grained non-porphyritic pink granites
	Intrusive contact		
Mesoproterozoic (1600 Ma ?)		Mafic intrusives	Metadolerites, gabbro, diorites
	Intrusive contact		
Paleo-Mesoproterozoic (1900–1400 Ma)	Shillong Group	Barapani Formation Tyrsad Formation	Boulder bed (?), quartzites, actinolite, schists, phyllites
~ ~ ~ ~ ~ ~ ~ ~ ~ ~ ~ ~	~Unconformity	~ ~ ~ ~ ~ ~ ~ ~ ~ ~	~ ~ ~ ~ ~ ~ ~ ~ ~ ~ ~ ~
Late Archean to Early Proterozoic (2670–2250 Ma)		Basement Gneissic Complex (BGC)	Granite gneiss, migmatites

[?]No absolute age is available for the metadolerites of the Shillong Basin. The age of these rocks are estimated from palaeomagnetic investigations and age of other rock associations from the Shillong Basin.

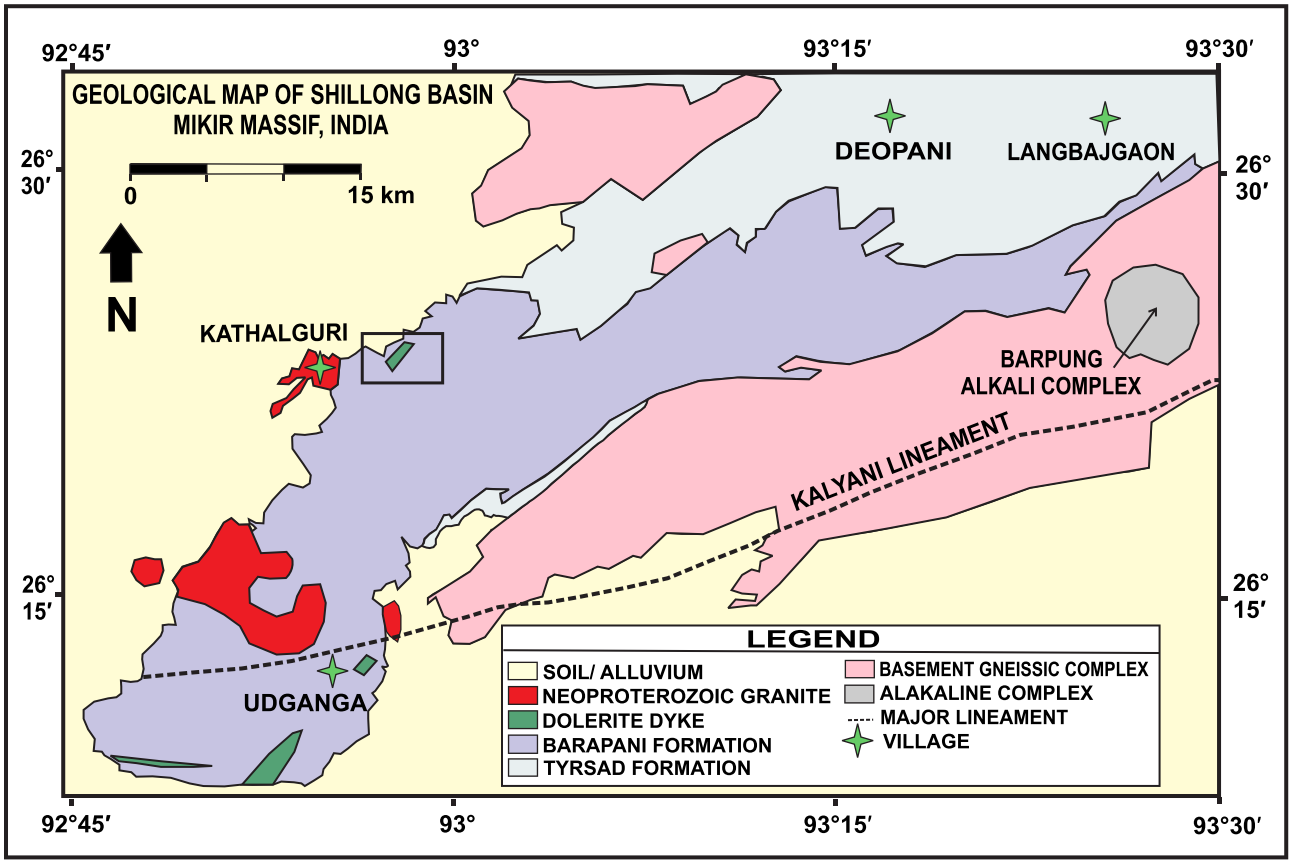

Figure 2. (Colour online) Regional geological map of Mikir Massif showing the study area within the black box (modified after Dhurandhar *et al.* 2019).

https://doi.org/10.1017/S0016756823000237 Published online by Cambridge University Press

Figure 3. (Colour online) Field photographs showing (a) a metadolerite hand specimen. (b–d) Quartzites of the Shillong Group share sharp contacts with the metadolerites or Khasi greenstones. (e, f) Closely spaced vertical joints crisscrossed by another set of joints at a higher angle (shown by yellow lines) and a set of conjugate joints (shown by white lines) were observed in metadolerites.

study has been carried out at a large quarry site near the Borjuri village spreading across an area of about 2 sq km (Fig. 2).

3. Field relationships

The Proterozoic mafic intrusives occur in the northwestern domain of the Mikir Massif near the Borjuri village of Nagaon district, Assam. These mafic rocks are basically melanocratic metadolerites (Fig. 3a). The metadolerites share sharp contacts with the quartzitic rocks of the Shillong Group (Fig. 3b-d). The metadolerites show variation in grain size. The rocks are relatively finer towards contact with the quartzites. The metadolerites and the metasedimentary quartzite sequence in the study area have a regional trend of NE-SW and a regional dip towards SE. The area is highly jointed and consists of two sets of prominent joints. The dominant regional joints are systematic, closely spaced joints striking N45°E. The regional joints are crisscrossed by another set of joints at a higher angle striking N30°W. A set of conjugate joints are also seen sporadically in the area (Fig. 3e, f).

4. Analytical methods

Mineral chemical analyses of the metadolerites were performed on polished thin-sections using a CAMECA SX 100 electron microprobe at Electron Microprobe Analyser Laboratory, Geological Survey of India, Faridabad (India). The analyses were carried out using an acceleration voltage of 15 kV and beam current of 10 nA with a beam diameter of ca. 1 μm. Standards used include periclase for Mg, wollastonite for Si and Ca, albite for Na, rhodonite for Mn, orthoclase for K, corundum for Al, apatite for P, hematite for Fe, metallic chromium and titanium for Cr and Ti, halite for Cl, metallic zinc for Zn, fluorite for F and barite for Ba. The error in major element concentrations is <1%, whereas the error on trace elements varied between 3 and 5%. For all the elements, Kα lines were analysed with a peak counting time of 10 s and a background counting time of 5 s. The corrections applied to the raw data were that of Pouchou and Pichoir (PAP) procedure (Pouchou & Pichoir, 1987).

The major oxides, trace elements and rare earth element (REE) analyses were carried out at the Wadia Institute of Himalayan

https://doi.org/10.1017/S0016756823000237 Published online by Cambridge University Press

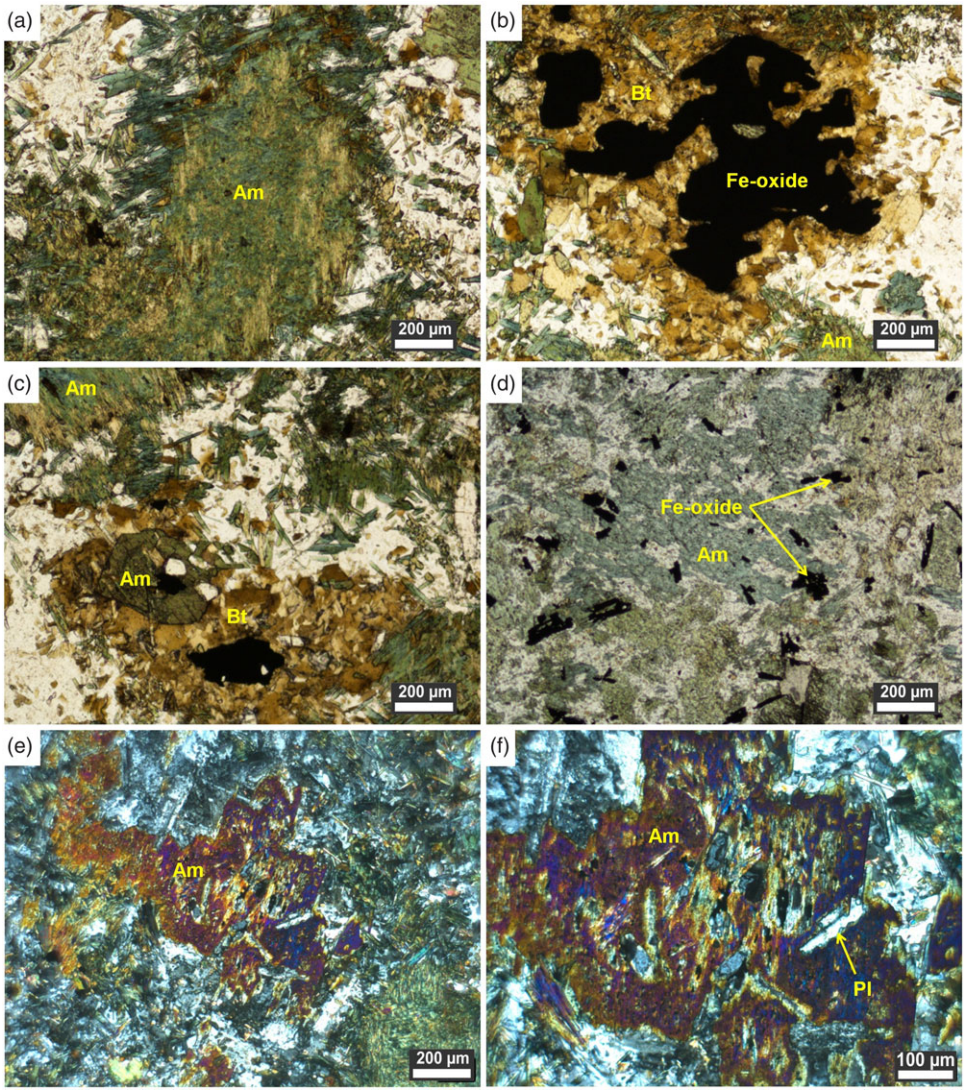

Figure 4. (Colour online) Representative photomicrographs of the metadolerites illustrating the mineral assemblages (a) plane-polarized light (PPL) images of secondary amphibole, (b, c) amphibole, biotite and Fe-oxide, (d) amphibole and Fe-oxide and (e, f) cross-polarized light (CPL) images of plagioclase laths embedded within secondary amphibole. Mineral abbreviations: Am, amphibole; Bt, biotite; Pl, plagioclase.

Geology, Dehradun (India). Major oxides and selected trace elemental analyses were performed using a Bruker S8 Tiger Sequential X-ray Spectrometer with Rh excitation source, following the processes explained by Saini *et al.* (2000). The operating conditions for major oxides were no filter, vacuum path and 20/40 kV; for trace elements, they were no filter, vacuum path and 55/60 kV. For major and minor oxides, the overall accuracy in relative standard deviation (RSD) percentage is <5%; for trace elements, it is <12%. The average precision is better than 2% (Saini *et al.* 2007). The ICP-MS analyses of the REEs were done using the equipment PerkinElmer SCIEX quadrapole type ICP-MS, ELAN DRC-e. For REE analysis, sample solutions were introduced into the argon plasma by means of a peristaltic pump and a cross flow nebulizer. Sample digestion and preparation of solutions were carried out following the procedures of Balaram *et al.* (1990). To minimize matrix effect, United States Geological Survey (BHVO-1, AGV-1) and Geological Survey of Japan (JB1-a, JP-1) samples were used as rock standards. RSD for most of the samples is better than 10%.

5. Results

5.a. Petrography

Petrographically, the metadolerites can be divided into medium-grained and coarse-grained varieties. However, mineralogically they are similar and dominantly consist of amphibole, biotite, plagioclase and minor amounts of chlorite, apatite, titanite and Fe-oxides. Amphibole, plagioclase and biotite were analysed by an electron microprobe to determine their compositions. Representative mineral chemical analyses of these minerals are presented in Supplementary Tables S1, S2 and S3.

The amphiboles are basically secondary phases after pyroxene and are medium to coarse-grained having an elongated prismatic habit and some occur as anhedral masses as well (Fig. 4a). On the amphibole classification diagram (Hawthorne *et al.* 2012), the amphiboles plot in the field of magnesio-hornblende and pargasite (Supplementary Fig. S1). Hence, the amphiboles can be classified as calcic-amphiboles. The Ca content of the amphiboles ranges from 1.57 to 1.95 *apfu* (atom per formula unit), Al^{iv} varies from

https://doi.org/10.1017/S0016756823000237 Published online by Cambridge University Press

1.49 to 1.72 *apfu*, $(Na+K)_A$ from 0.42 to 0.62 *apfu* and Mg# ranges from 0.37 to 0.42. The biotite grains are brown-coloured tabular crystals showing mottled birds-eye extinction (Fig. 4b, c). On the biotite classification diagram (Tischendorf *et al.* 1997), the biotites are classified as Fe-biotites (Supplementary Fig. S2). The Si value of biotite ranges from 6.28 to 7.10 *apfu*, total Al abundance ranges from 1.35 to 1.50 *apfu* and Fe+Mg values ranges from 2.45 to 2.70 *apfu*. On the $FeO+MnO–MgO–10TiO_2$ ternary diagram (Nachit *et al.* 2005), the analysed biotite crystals distinctly plot within the re-equilibrated biotite field (Supplementary Fig. S3), which suggests that biotite crystals in the studied rocks are secondary in nature. The plagioclase crystals generally occur as medium-grained, lamellar-twinned lath-shaped crystals. The analysed plagioclase grains are of oligoclase and andesine composition (An_{21} to An_{32}) (Supplementary Fig. S4). Minor acicular apatite grains and anhedral Fe-oxides occur as discrete mineral phases in the section (Fig. 4d).

Both the coarse-grained and medium-grained metadolerites show inequigranular, holocrystalline texture. Primarily, plagioclase laths are embedded within amphibole grains, which resemble an ophitic texture (Fig. 4e, f). There is a possibility that the amphiboles present are secondary minerals formed by the transformation from pre-existing pyroxene grains. This suggests that the mafic rocks have been influenced by metamorphism leading to the formation of secondary amphiboles.

5.b. Geochemistry

The major and trace element distributions of the Borjuri metadolerites are presented in Table 2. In general, for the geochemical classification of subvolcanic rocks for un-metamorphosed samples, the total alkali versus silica diagram is used (La Bas *et al.* 1986). However, the studied mafic rocks have undergone deformation and metamorphism. Hence, the immobile trace elements such as REEs and high field strength elements (HFSEs) are given more importance. The HFSE ratio of parent rocks is similar to that of the altered rocks (Finlow-Bates & Stumpfl, 1981; MacLean & Barrett, 1993). We have therefore adopted a classification diagram based on immobile elements, which is generally used for altered rocks. In the Zr/Ti versus Nb/Y discrimination diagram after Pearce (1996), all the studied samples plot in the field of basalt (Fig. 5a). The mafic rocks show tholeiitic trend in the (Na_2O+K_2O)-FeO^T-MgO or AFM (alkalis-iron-magnesium) plot (Fig. 5b; Irvine & Baragar, 1971). We have drawn a comparison of our data with known Indian occurrences of Proterozoic mafic rocks from the BVSs of CGGC: pillow basalts and dolerites after Ahmad *et al.* (2021) and dolerites after Gogoi (2022).

The primitive mantle-normalized multi-element diagram is shown in Figure 6a. The diagram exhibits distinct peaks at large ion lithophile elements (LILE) Rb, K and Pb, and noteworthy troughs at HFSEs Nb, Zr and Yb. The elevated concentrations of LILE in the rocks can be attributed to dehydration of the subducted slab and transportation of the LILE-rich fluids to the overlying mantle wedge (Saunders *et al.* 1980; Wilson & Davidson, 1984). The negative aberrations depicted by Nb and Yb can be ascribed to the subduction zone magmatic regime (Sheraton *et al.* 1990; Zhao *et al.* 1995). Chondrite-normalized REE diagram of the studied metadolerites displays elevated patterns for LREE ($(La/Yb)_N$=3.49–4.97; $(Gd/Yb)_N$=1.98–2.30)) and nearly flat patterns for HREE (Fig. 6b). Most of the samples exhibit positive europium anomaly (Eu/Eu*=0.99–1.13) indicating accumulation of plagioclase. The REEs displaying sub-parallel trends suggest that the rocks are cogenetic in nature. The trace and REE patterns of mafic rocks from the Shillong Basin are similar to those of mafic rocks from the BVSs, with the samples from the former displaying slightly enriched character (Fig. 6a, b).

5.c. Pressure and temperature estimates

For geothermobarometric studies, six pairs of mineral chemical data of plagioclase and amphibole were selected from the metadolerites. Various researchers have proposed several methods (Blundy & Holland, 1990; Holland & Blundy, 1994; Anderson & Smith, 1995; Anderson, 1996) for geothermobarometry calculations. Amphiboles are crucial minerals for geothermobarometry as they are combinedly affected by parameters such as pressure, temperature and oxygen fugacity. From experimental and field studies regarding the depth of emplacement of plutons, it is seen that the Al content of amphibole is considered a function of pressure and temperature (Hollister *et al.* 1987; Thomas & Ernst, 1990; Blundy & Holland, 1990; Schmidt, 1992; Anderson & Smith, 1995).

The metamorphic P-T conditions were estimated using the amphibole-plagioclase geothermobarometry. To calculate pressure, we have used the formulation of Al-in-hornblende barometer by Anderson & Smith (1995). The errors associated with the Al-in-hornblende barometer are ± 0·6 kbar. The pressure obtained for the samples varies between 7 and 8 kbar (Supplementary Table S4). Holland & Blundy (1994) proposed two geothermometers. One applies to quartz-bearing igneous rocks (edenite + 4 quartz = tremolite + albite), while the other is for both quartz-bearing and quartz-free igneous rocks (edenite + albite = richterite + anorthite). For our samples, compositions of amphibole along with coexisting plagioclase were used for temperature calculations. The calculation was carried out with the help of amphibole-plagioclase geothermometer (edenite-richterite thermometer) after Holland & Blundy (1994). The errors associated with the thermometer are ± 40°C. The temperature of the samples ranges from 633°C to 703°C with an average of 664°C (Supplementary Table S4). In the calcic amphibole discrimination diagram (Supplementary Fig. S5) by Fleet & Barnett (1978), the amphiboles distinctly plot in the low-pressure metamorphic field. In the temperature–pressure diagram, the estimated temperature and pressure of the metadolerites plot in the amphibolite facies and medium P-T zone (Supplementary Fig. S6).

6. Discussion

6.a. Post-crystallization alteration and crustal contamination

The field as well as petrographic observations shows post-crystallization alteration effects in the metadolerites of Borjuri area. Amphibole, biotite and chlorite observed under a microscope are secondary minerals that have formed from the replacement of primary Fe-Mg minerals, such as pyroxene. Isochemical and volume-to-volume replacement are responsible for the replacement of original pyroxene by amphiboles which do not bring about any changes in the original igneous textures (Redman & Keays, 1985). The occurrence of such secondary metamorphic minerals helps to ascertain the degree of alteration. Other than the petrographic study, the extent of post-magmatic alteration processes can also be evaluated with the help of Harker variation diagrams. A series of binary variation diagrams (Fig. 7) of selected major and trace elements have been plotted against SiO_2, and the observations

https://doi.org/10.1017/S0016756823000237 Published online by Cambridge University Press

Table 2. Major oxides (wt %), trace and rare earth elements (ppm) composition of the metadolerites of Borjuri from Mikir Massif part of Assam-Meghalaya Gneissic Complex

Sample	MD6	MD9	MD10	MD11	MD12	MD13	MD16	MD17	MD18	MD19
Major oxide (wt %)										
SiO_2	44.59	41.45	40.49	43.65	44.06	45.44	45.72	45.08	44.95	45.65
TiO_2	2.96	3.3	3.43	3.19	2.83	3.03	2.88	2.65	2.61	2.93
Al_2O_3	14.15	13.58	13.78	13.95	13.34	13.96	13.66	13.78	13.49	13.27
Fe_2O_3	15.71	18.2	19.78	16.16	15.92	16.7	15.66	16.37	16.63	15.68
MnO	0.21	0.28	0.25	0.25	0.24	0.23	0.22	0.2	0.21	0.22
MgO	6.93	6.83	7.16	6.48	6.79	6.55	7.1	7.38	7.28	7.15
CaO	9.34	6.43	5.1	6.7	8.31	8.82	8.49	8.74	8.8	7.84
Na_2O	2.36	1.56	1.35	2.05	2.04	2.66	2.68	2.26	2.34	2.5
K2O	1.13	4.52	5.23	4.02	3.04	1.15	1.29	1.68	1.56	1.32
P_2O_5	0.44	0.44	0.46	0.47	0.5	0.54	0.52	0.45	0.46	0.48
LOI	0.76	2.18	2	2.2	1.66	0.63	1.05	1.14	0.99	1.76
SUM	98.58	98.77	99.03	99.12	98.73	99.71	99.27	99.73	99.32	98.8
Mg #	46.62	42.63	41.75	44.26	45.8	43.71	47.31	47.17	46.44	47.45
Trace elements (ppm)										
Ba	409	669	808	650	562	364	406	420	431	403
Cr	122	135	135	105	84	77	78	99	102	78
V	303	301	296	293	278	289	286	291	267	297
Sc	31	27	24	29	31	28	27	25	29	29
Co	67	74	74	67	65	71	69	69	77	70
Ni	117	129	122	121	122	123	128	129	124	125
Cu	63	8	7	7	63	74	65	47	43	52
Zn	123	224	228	200	164	127	134	119	124	127
Ga	17	22	20	21	16	18	17	17	17	18
Pb	5	6	5	7	6	5	6	6	5	6
Th	2.5	1.5	1	0.7	1.6	1.2	1.8	1.1	BDL	1.7
Rb	23	192	222	169	107	32	27	62	46	47
U	0.8	0.5	0.5	0.7	0.6	0.7	0.8	0.8	0.9	0.7
Sr	337	214	228	258	244	295	312	335	341	289
Y	39	62	64	56	51	44	44	43	43	46
Zr	139	158	167	173	166	168	162	140	150	168
Nb	11	12	14	14	12	12	12	11	11	13
REE (ppm)										
La	18.48	15.21	23.59	28.22	27.35	25.41	28.36	14.99	21.58	20.35
Ce	42.93	39.27	58.87	70.26	67.62	65.2	62.2	37.2	50.07	54.67
Pr	6.53	6.09	8.21	9.68	9.37	8.72	9.38	5.44	7.28	7.31
Nd	29.93	27.95	36.94	43.42	42.46	39	40.92	24.75	32.14	32.6
Sm	7.03	7.03	9.22	10.48	10.13	9.22	9.77	5.91	7.81	8.27
Eu	2.74	2.64	3.47	3.94	3.81	3.27	3.28	2.26	2.7	2.85
Gd	7.82	8.27	10.13	11.75	11.46	10.45	10.56	6.73	8.49	9.12
Tb	1.12	1.26	1.53	1.75	1.72	1.56	1.55	1.02	1.25	1.37
Dy	6.38	7.35	8.92	9.99	9.45	8.73	8.79	5.73	7.16	7.77

(*Continued*)

https://doi.org/10.1017/S0016756823000237 Published online by Cambridge University Press

Table 2. (*Continued*)

Sample	MD6	MD9	MD10	MD11	MD12	MD13	MD16	MD17	MD18	MD19
Ho	1.33	1.56	1.91	2.06	1.97	1.8	1.87	1.22	1.49	1.62
Er	3.38	3.87	4.93	5.17	5.13	4.46	4.73	3.04	3.87	4.18
Tm	0.47	0.52	0.69	0.7	0.71	0.62	0.64	0.41	0.52	0.56
Yb	2.81	3.13	4.23	4.26	4.29	3.85	4.09	2.47	3.3	3.5
Lu	0.4	0.43	0.59	0.61	0.62	0.56	0.59	0.36	0.47	0.51
SUM	131.35	124.59	173.24	202.27	196.08	182.83	186.72	111.53	148.13	154.67
$(La/Yb)_N$	4.72	3.49	4	4.75	4.58	4.74	4.97	4.35	4.69	4.17
$(Gd/Yb)_N$	2.3	2.18	2.98	2.28	2.21	2.25	2.14	2.25	2.12	2.15
Ba/Nb	37.18	53.95	56.9	47.1	46.07	30.08	33.28	38.89	37.81	31.98
La/Nb	1.68	1.23	1.66	2.04	2.24	2.1	2.32	1.39	1.89	1.61
Zr/Ba	0.34	0.24	0.21	0.27	0.3	0.46	0.4	0.33	0.35	0.42
Eu/Eu*	1.13	1.06	1.1	1.08	1.08	1.02	0.99	1.09	1.01	1

LOI, loss on ignition; BDL, below detection limit.

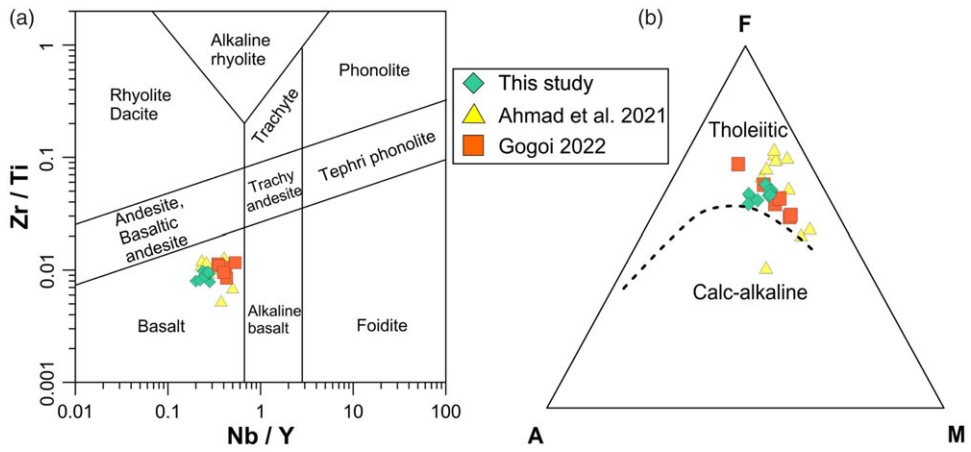

Figure 5. (Colour online) (a) Geochemical classification diagram based on immobile trace elements (after Pearce, 1996) and (b) AFM diagram displaying tholeiitic nature of magma for the metadolerites of Borjuri (after Irvine & Baragar, 1971). Data used for comparison are from Proterozoic mafic rocks of Bathani volcano-sedimentary sequence: Ahmad *et al.* (2021) and Gogoi (2022).

show positive, negative and scattered trends. The elements CaO, Na_2O, P_2O_5 and Sr show positive trends in a linear or non-linear way, which is suggestive of the accumulation of plagioclase and apatite in the evolving magma. However, with an increase in SiO_2, the elements Fe_2O_3, TiO_2, K_2O, Rb, Cr and Y all show negative trends. This is indicative of the fractionation of amphibole, biotite, clinopyroxene, titanite and Fe-Ti oxides in the evolving magma. The positive and negative trends displayed by these major and minor elements suggest near primary magmatic characteristics. On the other hand, the elements MgO and Al_2O_3 show plots of scattered nature, which decipher post-crystallization alteration effects or the post-magmatic mobility of these elements.

Mantle-derived mafic magmas are prone to crustal assimilation during ascent or when emplaced in crustal magma chambers (Mohr, 1987; Pe-piper *et al.* 2003). It is therefore crucial to assess the effects of crustal contamination on the chemical composition of the primary mafic magma. Elemental ratios such as Ba/Nb, Ti/Y, La/Yb, Ba/Zr, La/Sm, Zr/Y, Nb/La, Nb/Th and Nb/Y are frequently used to evaluate crustal assimilation in mafic rocks (Rollinson, 1993). Trace-element ratio plots for the Borjuri metadolerites are presented in Figure 8a–d. Plots show that the studied metadolerites plot away from the mantle array, which likely suggests an influence of crustal assimilation (Fig. 8a, b). The Nb/La versus SiO_2 and Nb/Th versus Nb/La diagrams also suggest a crustal contamination in the samples (Fig. 8c, d).

6.b. Magmatic evolution

Mafic rocks derived from the lithospheric mantle have higher LILE and LREE element abundances and lower HFSE than those generated by the asthenospheric mantle melting. As a result of these variations in elemental abundances between the asthenospheric and lithospheric mantle, an arrangement of HFSE–LREE ratios is useful for understanding the source of mantle-derived rocks. The Zr/Ba values are being routinely used to differentiate between asthenospheric (Zr/Ba > 0.5) and lithospheric sources (Zr/Ba = 0.3–0.5) (Ormerod *et al.* 1988; Menzies *et al.* 1991). The Zr/Ba range of the studied samples varies from 0.21 to 0.46

https://doi.org/10.1017/S0016756823000237 Published online by Cambridge University Press

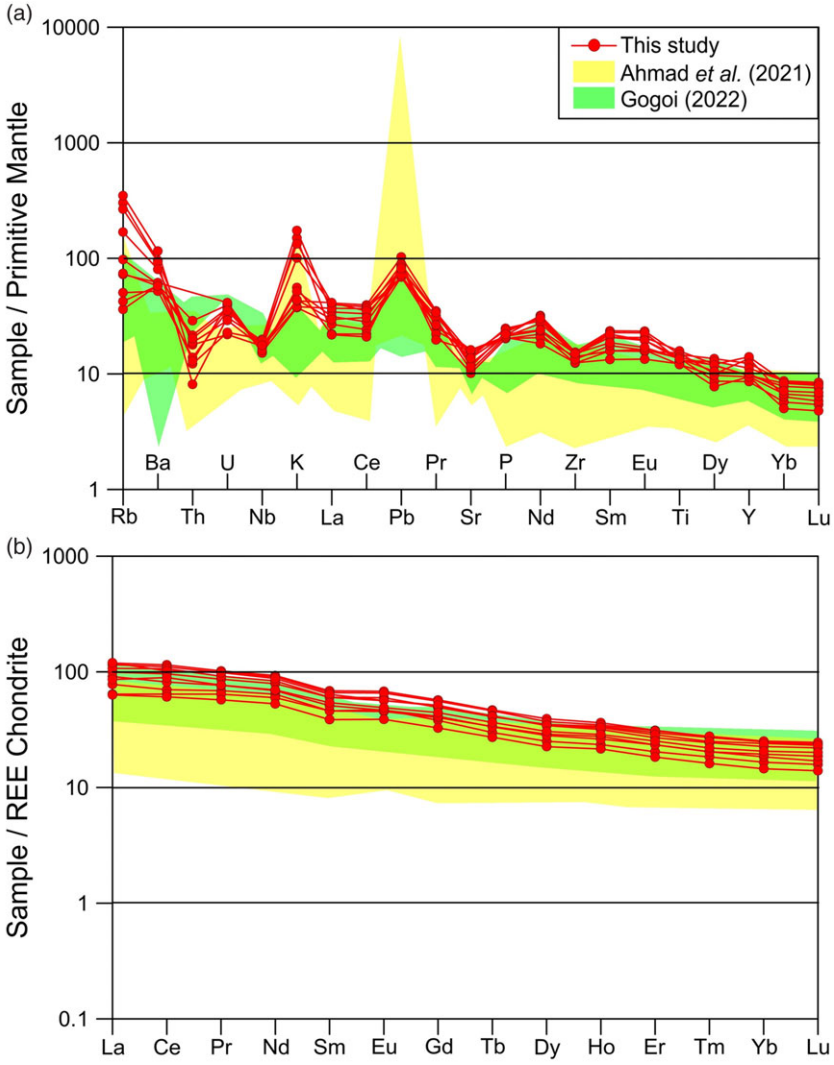

Figure 6. (Colour online) (a) Primitive mantle-normalized multi-element diagram (normalizing values after Sun & McDonough, 1989) and (b) chondrite-normalized rare earth element patterns (normalizing values after Boyton, 1984) for the metadolerite samples of Borjuri. For comparison purpose, trace element data in yellow and green patterns are plotted from Ahmad *et al.* (2021) and Gogoi (2022) respectively.

indicating the involvement of the lithospheric mantle. Moreover, the elemental ratio of La/Nb of the Borjuri metadolerites ranges from 1.23 to 2.32. This is comparable to the lithospheric mantle where La/Nb > 1 (Fitton *et al.* 1988; Thompson & Morrison, 1998). The ratio La/Nb also therefore suggests an origin from the lithospheric mantle for the metadolerites. As HFSEs like Nb are depleted in the lithospheric mantle with respect to the LREEs, low Nb/La implies a lithospheric mantle origin and higher Nb/La suggests an OIB-like asthenospheric mantle source. The plot of (La/Yb) versus (Nb/La) (Smith *et al.* 1999) further confirms the origin of the metadolerites from lithospheric and mixed lithospheric–asthenospheric mantle sources (Fig. 9a).

The trace elemental signatures such as enrichment of LILE with respect to HFSE and negative Nb anomaly are all aspects of subduction-related mantle metasomatism. Generally, the enrichment of mantle source region can be ascribed to metasomatism by (1) fluxing of slab-derived fluids obtained from the dehydration of oceanic crust (Hawkesworth *et al.* 1993; Turner *et al.* 1997) and (2) addition of hydrous melts of subducted sediments (Peacock *et al.* 1994; Hawkesworth *et al.* 1997) or of the MORB segment of the slab (Peacock *et al.* 1994; Stern & Kilian, 1996). The distribution and variability of elements such as REE, Th and Ba provide valuable constraints for identifying the role of slab-derived fluids and slab-derived melts in mantle metasomatism (Spandler & Pirard, 2013; Guo *et al.* 2015). In the Th/Sm versus Th/Ce plot (Fig. 9b), the metadolerites illustrate a sediment-input trend indicative of sediment-related melt enrichment. The vertical and horizontal trends shown by the ratio plots of Rb/Y versus Nb/Y (Fig. 9c) and Nb/Zr versus Th/Zr (Fig. 9d), respectively, indicate fluid-related enrichment of the mafic magma. Source enrichment by fluids from the subducted slab is also supported by high Ba/Nb (> 28; Fitton *et al.* 1988). Ba/Nb ratio of the studied metadolerites ranges from 30.08 to 56.90. Fluids obtained from the subducted slab will modify the overlying mantle wedge geochemically. It will also lower the peridotite solidus to generate magmas (Stolper & Newman, 1994; Grove *et al.* 2002). Trace elemental geochemical attributes of the metadolerites of Borjuri strongly suggest derivation from a fluid-enriched lithospheric mantle source in a subduction regime.

A petrogenetic model based on Ni versus Zr was used for evaluating the lherzolite mantle composition. It is evident from the Ni versus Zr plot (Condie *et al.* 1987) that the metadolerites are products of a primary magma generated by 6%–10% melting of a lherzolite mantle source (Fig. 10a). REE ratios and their abundances

https://doi.org/10.1017/S0016756823000237 Published online by Cambridge University Press

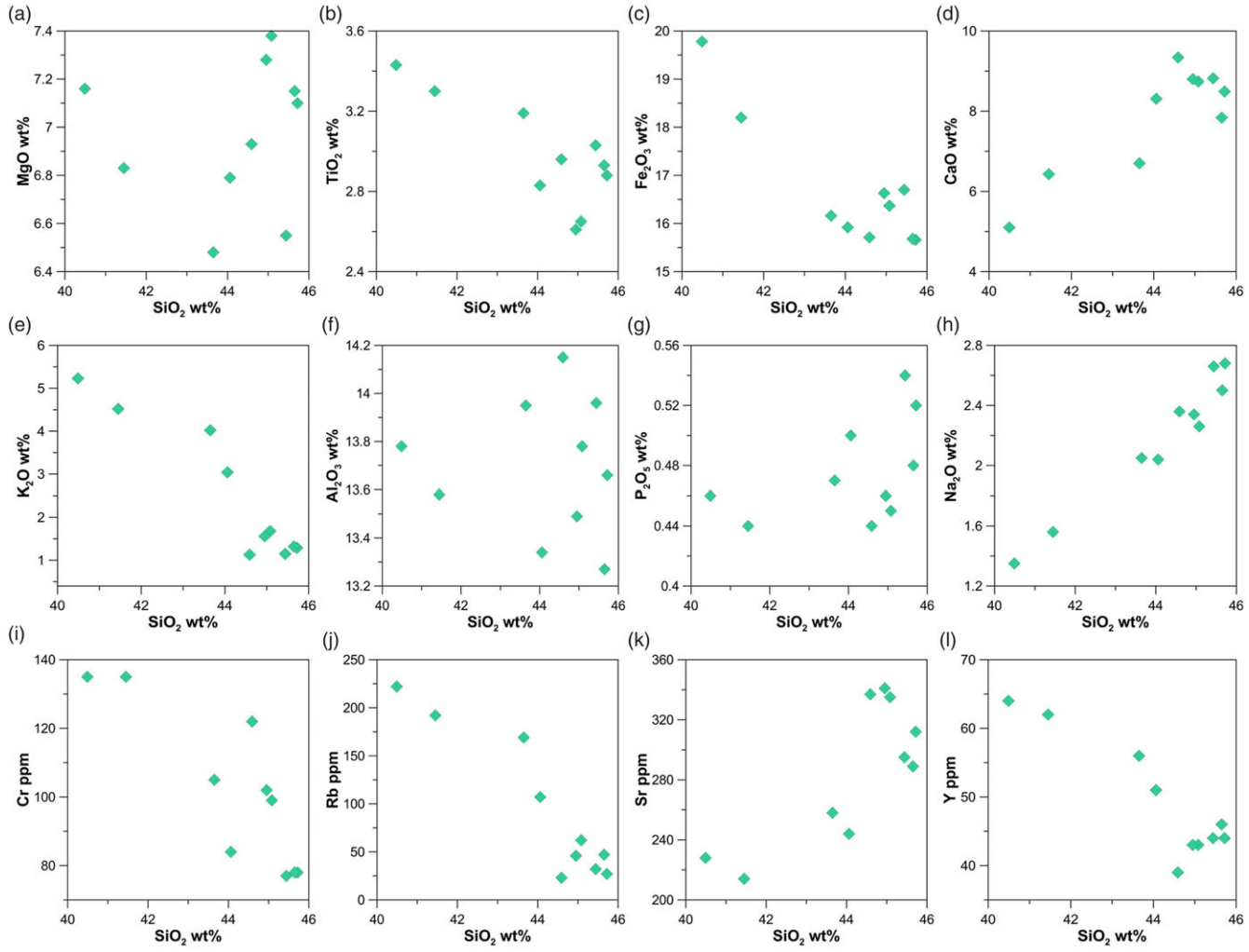

Figure 7. (Colour online) Bivariate diagrams of (a–h) major elements versus SiO_2 and (i–l) selected trace elements versus SiO_2.

(e.g. Sm/Yb and La/Yb) are extensively used to determine the source of mafic magmas and the degree/variation of mantle melting (McKenzie & O'Nions, 1991; Su *et al.* 2012). In the Sm/Yb versus La/Yb diagram, the studied samples plot below or near the spinel + garnet lherzolite (50:50) melting curve with primitive mantle as the initial composition (Fig. 10b). Here, the Sm/Yb values are lower than that of the garnet lherzolite melting curve and higher than that of the spinel lherzolite melting curve. Therefore, it can be inferred that the parental mafic magma for metadolerites was obtained from a mantle source incorporating spinel + garnet lherzolite. Moreover, the Sm/Yb versus La/Yb plot indicates an approximately 6%–10% partial melting of mantle lherzolite was necessary for the generation of parental magma of the metadolerites. Thus, from the trace element ratio plots it is evident that the parental magma of the metadolerites from Borjuri area was produced by 6%–10% melting of the lherzolite mantle source.

6.c. Geotectonic framework

Rocks of basaltic composition are ubiquitous in every tectonic environment. They are geochemically sensitive to the changes in the geotectonic framework. Thus, the geochemical signature of basaltic rocks is commonly used to discriminate tectonic settings. The metadolerites of Borjuri area show high LREE/HREE and LILE/HFSE ratios, which are distinguishing traits of magmas produced in subduction zones (Hawkesworth *et al.* 1993; Gorton & Schandl, 2000). In the Th/Yb versus Nb/Y tectonic discrimination diagram (Pearce, 2008), composition of the metadolerites clusters near E-MORB composition (Fig. 11a) displaying resemblance to back-arc basalts and dolerites of the BVSs (Ahmad *et al.* 2021; Gogoi, 2022). Furthermore, fluid immobile elements such as Zr, Ti, V and Y, which are independent of secondary processes (e.g. weathering and metamorphism), help in evaluating the tectonic setting of altered basic rocks. In the Ti/100-Zr-Yx3 ternary diagram (after Pearce & Cann, 1973), the metadolerites display mixed signatures of mid-oceanic ridge basalt, island arc tholeiites and calc-alkali basalts (Fig. 11b). The observed hybrid mixture between mid-oceanic ridge basalt and island arc tholeiites for the studied mafic rocks can be associated with back-arc basin basalts (Pearce & Peate, 1995; Pearce & Stern, 2006). In the Ti/Zr versus Zr (Fig. 11c) and V/Ti versus Zr (Fig. 11d) discrimination diagrams after Woodhead *et al.* (1993), the mafic rocks distinctly plot in the field of back-arc basin. Thus, it can be inferred that the parental magmas responsible for the generation of the metadolerite intrusives were produced in a back-arc extensional basin associated with subduction dynamics. Our data show similar geochemical characteristics to the known occurrences of mafic rocks from the BVSs.

https://doi.org/10.1017/S0016756823000237 Published online by Cambridge University Press

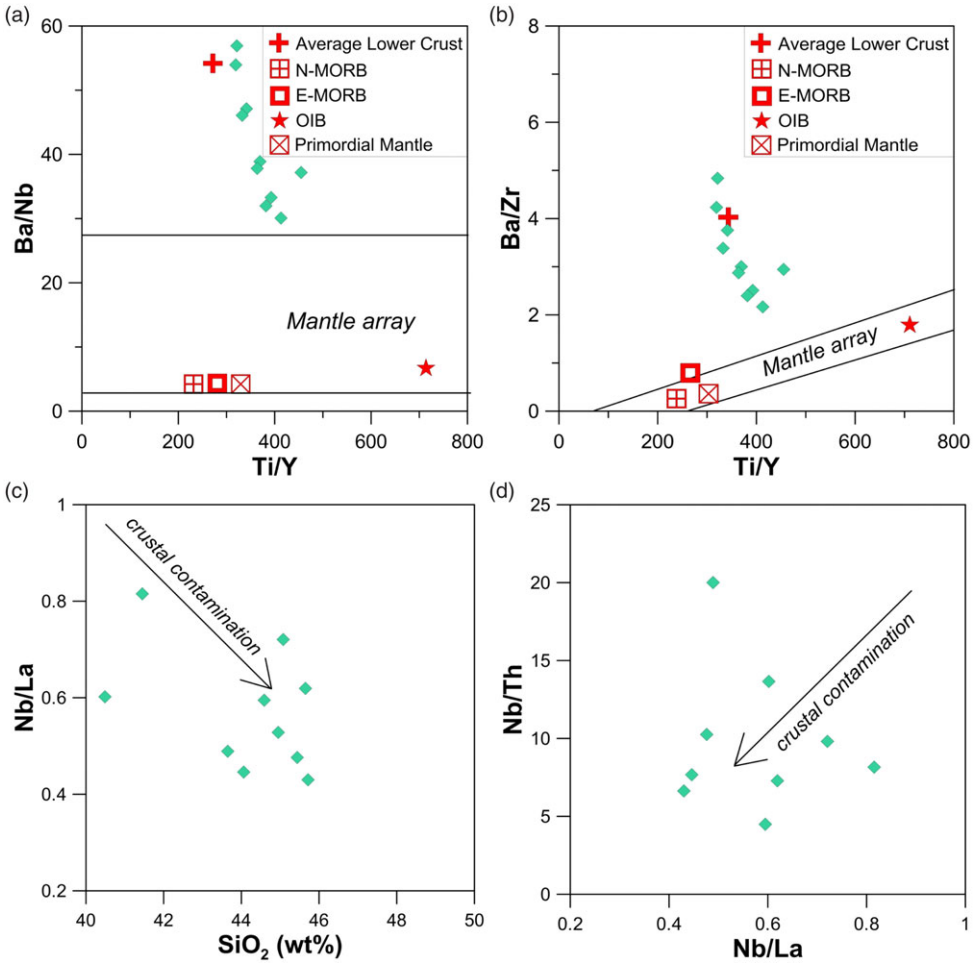

Figure 8. (Colour online) (a) Ti/Y versus Ba/Nb, (b) Ti/Y versus Ba/Zr, (c) Nb/La versus SiO_2 and (d) Nb/La versus Nb/Th variation diagrams of the mafic rocks of Borjuri.

6.d. Geodynamic implications

The Shillong Basin is an integral unit of AMGC that developed in the east-central part of the Meghalaya plateau and continued up to the Mikir Massif. This NE-SW interior basin is believed to have originated due to a thermal event followed by subsidence in a tensional stress regime (Nandy, 2001). The initiation of sedimentation in the basin commenced as early as 1900 Ma and continued till 1400 Ma (zircon dates of quartzites by Bidyananda & Deomurari, 2007). The metasedimentary province of Shillong Basin is intruded by several mafic and felsic dykes and sills. These mafic units, which have been subjected to amphibolite-facies metamorphism, occur in close association with the quartzites of the Shillong Group of rocks in the Mikir Massif (Fig. 3b-d). In this study, we attempt to give the tectonic framework responsible for the formation of the Shillong Basin. The geochemical signatures of the metadolerites presented in this work indicate a subduction zone setting for the generation of these rocks induced by fluid flux melting of the lithospheric mantle in a back-arc region. This implicates that the Shillong Basin represents a back-arc rift basin.

Recorded geochronological evidence suggests that AMGC has undergone Columbian, Grenvillian and Pan-African magmatic events (Yin *et al.* 2010; Chatterjee *et al.* 2011; Kumar *et al.* 2017; Gogoi *et al.* 2019). Shreds of evidence of such events from AMGC establish its involvement in the amalgamation and breakup of Columbia, Rodinia and Pangea. The Paleo-Mesoproterozoic felsic magmatism of the AMGC (Bidyananda & Deomurari, 2007; Yin *et al.* 2010; Kumar *et al.* 2017; Gogoi *et al.* 2019; Doley *et al.* 2022) is comparable to the Aravalli Belt of northwest India (Kaur *et al.* 2013), Eastern Ghats Mobile Belt of southeast India (Dobmeier *et al.* 2006), MMB of central India (Bora *et al.* 2013) and CGGC (Ray Barman *et al.* 1990; Ray Barman & Bishui, 1994; Acharyya, 2003; Hossain *et al.* 2007; Saikia *et al.* 2017; Gogoi, 2022). On drawing a comparison between the geochemical trends shown by the metadolerites of Shillong Basin and mafic rocks of BVSs, it is clear that the similarity is very significant. Moreover, in the present study it is noted from field observations that the joints present in the metadolerites show a trend of NE-SW and a dip towards SE which is directly comparable to the regional trend of CITZ (ENE-WSW). From a comparative analysis of our geochemical data, similar lithological and structural frameworks and associated geological dates given by previous authors, we envisage that the Shillong Basin is the eastern continuation of the BVSs and MMB of the CITZ (Fig. 12).

In various hypothesized models, the Greater Indian Landmass has been an essential element in the build-up of the Columbia supercontinent (Zhao *et al.* 2002; Hou *et al.* 2008; Pesonen *et al.* 2012; Zhang *et al.* 2012; Pisarevsky *et al.* 2013; Bhowmik, 2019; Chattopadhyay *et al.* 2020; Sequeira *et al.* 2022). On the basis of previous literatures, it can be deduced that Columbia supercontinent assembled during 1900–1600 Ma and fragmented at around 1500–1200 Ma (Evans, 2013). An even wider time span for tectonic

https://doi.org/10.1017/S0016756823000237 Published online by Cambridge University Press

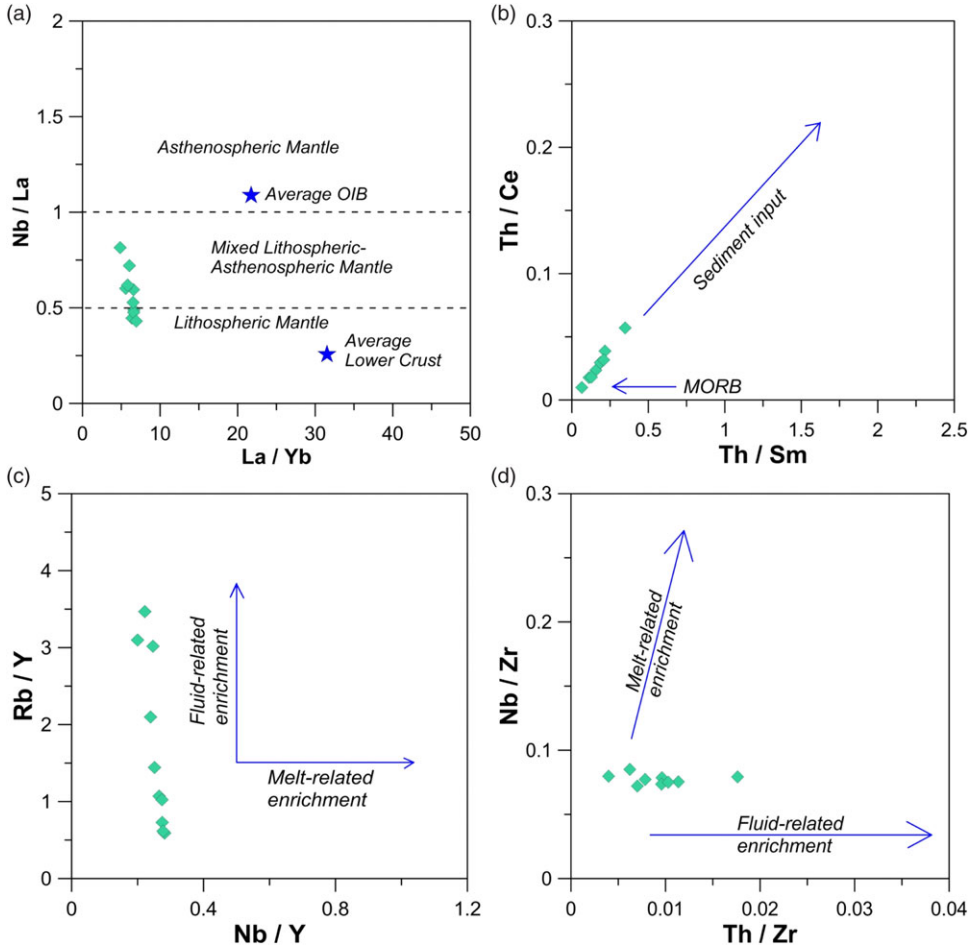

Figure 9. (Colour online) (a) La/Yb versus Nb/La (Smith *et al*. 1999) plot showing lithospheric and mixed lithospheric mantle source for Borjuri mafics. (b) Th/Sm versus Th/Ce plot of the Borjuri mafics shows the input of subducted sediment. (c) Nb/Y versus Rb/Y and (d) Nb/Zr versus Th/Zr, indicating fluid-related enrichment in Borjuri mafics.

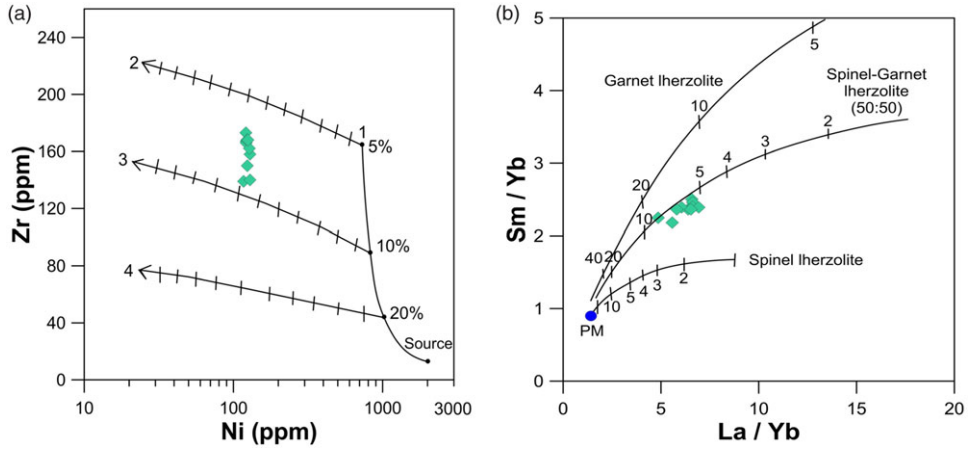

Figure 10. (Colour online) Plots for the metadolerites of Borjuri (a) Ni versus Zr petrogenetic model for a lherzolite mantle composition. Curve 1 signifies batch melting at 1500 °C (1 atm. equivalent) with percentages along the line representing degree of partial melting. Curves 2, 3 and 4 demonstrate olivine fractionation with elimination of olivine marked in 5% increments (after Condie *et al*. 1987). (b) La/Yb versus Sm/Yb diagram where the Borjuri metadolerites cluster near the spinel+garnet lherzolite curve (after Liu *et al*. 2014). Abbreviation: PM, primitive mantle.

history of the Columbia supercontinent, that is, ca 2100–1800 Ma for its amalgamation, 1800–1600 Ma for intracontinental rifting and 1300–1200 Ma for break-up, have been considered (Saha *et al*. 2016; Wang *et al*. 2019; Meert & Santosh, 2022). A large number of literatures are available regarding the position of Indian subcontinent within the Columbia supercontinent. India was placed near Laurentia and the North China Craton by Hou *et al*. (2008), while Zhang *et al*. (2012) have placed it adjacent to

https://doi.org/10.1017/S0016756823000237 Published online by Cambridge University Press

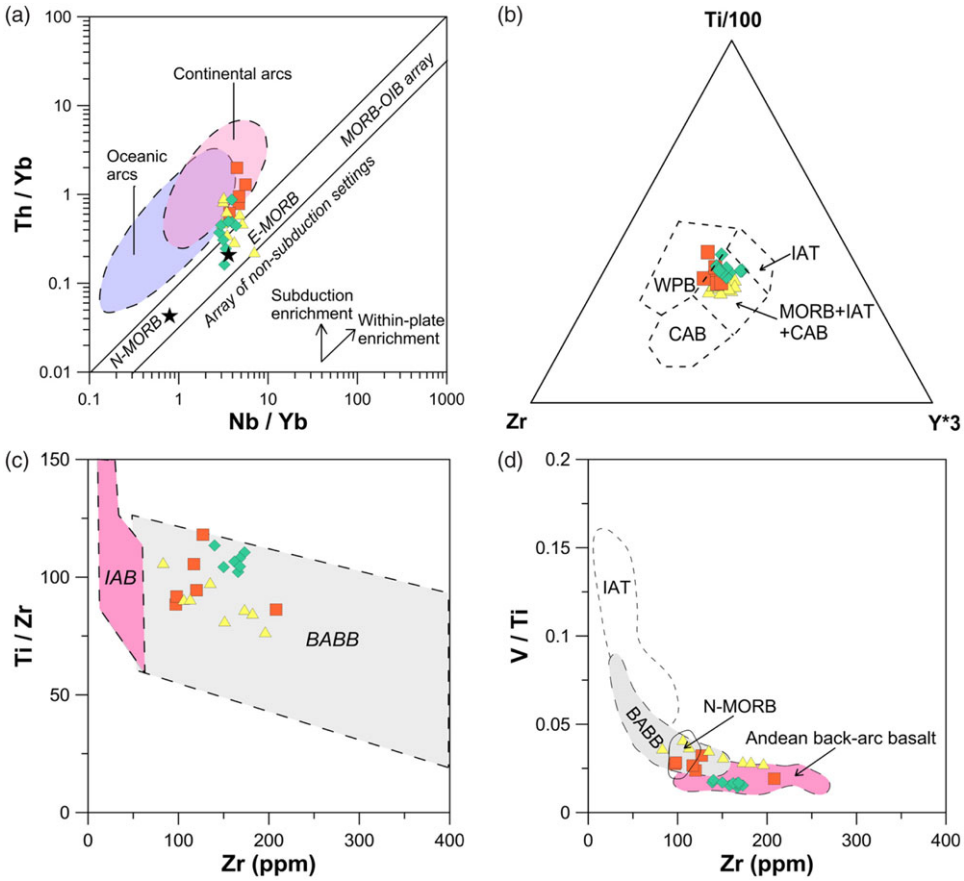

Figure 11. (Colour online) Tectonic discrimination diagrams for the Borjuri metadolerites. (a) Nb/Yb versus Th/Yb plot after Pearce (2008). (b) Ti/100-Zr-Yx3 ternary diagram after Pearce & Cann (1973). (c) Ti/Zr versus Zr after Woodhead *et al.* (1993). (d) Zr versus V/Ti after Woodhead *et al.* (1993). Field of Andean back-arc basalt is taken from Espanon *et al.* (2014). Abbreviations: BABB, Back-arc basin basalt; CAB, Calc-alkali basalts; IAB, Island-arc basalt; IAT, Island-arc tholeiites; MORB, Mid-oceanic ridge basalt; WPB, Within plate basalt. Symbols as in Figure 5.

Australia, and Pisarevsky *et al.* (2013) have positioned India next to the Sarmatia margin of Baltica. Thus, India's position in Columbia reconstructions has largely remained dubious due to inadequate geological and geochronological data. During Columbia formation, the northern and southern Indian blocks merged to form a single continental block, that is, the Greater Indian Landmass. Thus, India was not a single continental block until the amalgamation of Columbia (Saikia *et al.* 2017). To get a closer outlook on the assembly, configuration and breaking up of the Greater Indian Landmass in relation to Columbia supercontinent, it is necessary to look for a continuation of mobile belts similar to CITZ in other continental blocks. Identifying Paleo-Mesoproterozoic mobile belt with an associated back-arc rift basin will allow us to position the hypothesized proto-continental blocks in the hypothetical supercontinental models.

7. Conclusions

The AMGC is exemplary of a number of magmatic events which have led to many felsic and mafic intrusives within the basement gneisses as well as the Shillong Group of rocks. The studied metadolerites related to the Khasi greenstones are found as intrusive in contact with quartzites of the Borjuri area in the Mikir Massif. These metadolerites have undergone metamorphism reaching amphibolite facies conditions with estimated pressure and temperature of 7–8 kbar and 664 °C, respectively. The studied mafic rocks depict well-preserved signatures that define the geotectonic framework of a subduction zone setting, more specifically a back-arc extensional setting. Comparing geochemical data of the metadolerites and taking into consideration structural affiliations along with available geochronological dates, marked similarity is seen between the Shillong Basin of AMGC and BVSs of CGGC. Thus, we can conclude that the Shillong Basin is the eastern extension of the BVSs and also MMB of the CITZ.

Supplementary material. To view supplementary material for this article, please visit https://doi.org/10.1017/S0016756823000237

Acknowledgements. Bibhuti Gogoi acknowledges the DST-SERB grant vide Project No. CRG/2020/002635. Pallabi Basumatary acknowledges the CSIR-JRF fellowship No. 09/1236(11154)/2021-EMR-I. We would like to express our sincere gratitude to three anonymous reviewers for their insightful and constructive comments. We thank Dr. Sarah Sherlock for editorial handling of the manuscript. Useful suggestions by Dr. Amiya Baruah are gratefully acknowledged.

Competing interests. The authors declare that in this present work there is no conflict of interests.

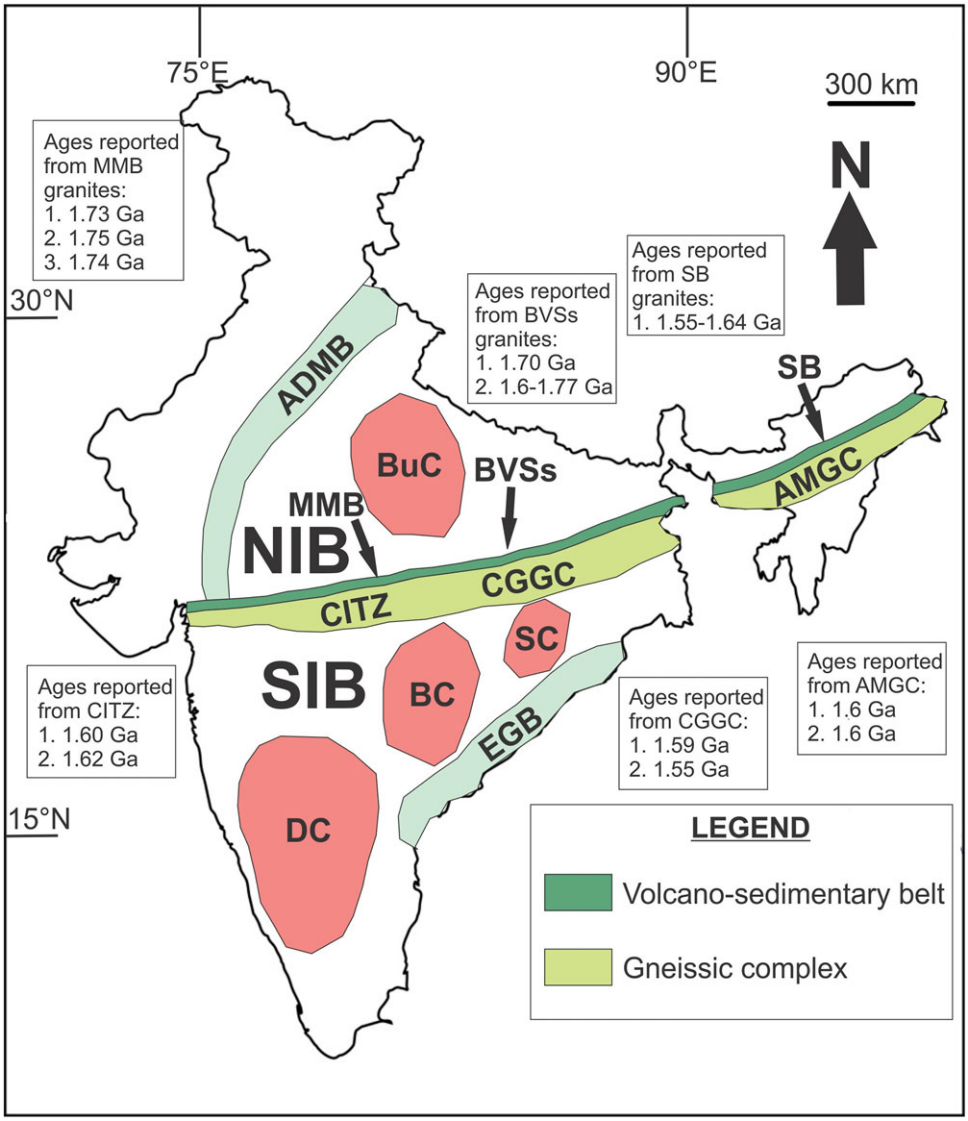

Figure 12. (Colour online) Map of Indian subcontinent displaying the ENE-WSW-trending Central Indian Tectonic Zone (CITZ), Chotanagpur Granite Gneiss Complex (CGGC) and Assam-Meghalaya Gneissic Complex (AMGC) (modified after Saikia *et al*. 2017). This continuous mobile belt demarcates the boundary between the North Indian Block (NIB) from the South Indian Block (SIB) (Acharyya 2003; Bhandari *et al*. 2011; Chatterjee & Ghose, 2011; Rekha *et al*. 2011; Bhowmik *et al*. 2012). The NIB comprises of the Bundelkhand Craton (BuC), whereas the SIB is a union of the Dharwar Craton (DC), the Singhbhum Craton (SC) and the Bastar Craton (BC). The Aravalli Delhi Mobile Belt (ADMB) and the Eastern Ghats Belt (EGB) are also shown. Two volcano-sedimentary sequences of CITZ, namely Mahakoshal Mobile Belt (MMB) and its eastern continuation Bathani volcano-sedimentary sequence (BVSs), are shown. The present study projects the Shillong Basin of AMGC as the eastern continuation of the BVSs. The ages reported from the MMB are taken from: 1) Sarkar *et al*. (1998); 2) Bora *et al*. (2013); 3) Yadav *et al*. (2015). The ages reported from the BVSs are taken from: 1) Chatterjee & Ghose (2011); 2) Saikia *et al*. (2017, 2019). The ages reported from the Shillong Basin are taken from: 1) Gogoi *et al*. (2019). The ages reported from the CITZ are taken from: 1) Bhandari *et al*. (2011); 2) Bhowmik *et al*. (2011). The ages reported from the CGGC are taken from: 1) Pandey *et al*. (1986); 2) Chatterjee *et al*. (2008). The ages reported from the AMGC are taken from: 1) Chatterjee *et al*. (2007); 2) Yin *et al*. (2010).

References

Acharyya SK (2001) Geodynamic setting of the Central Indian Tectonic Zone in central, eastern and north eastern India. *Geological Survey of India, Special Publication* **64**, 17–35.

Acharyya SK (2003) The nature of Mesoproterozoic central Indian tectonic zone with exhumed and reworked older granulites. *Gondwana Research* **6**, 197–214.

Ahmad M and Wanjari N (2009) Volcano-Sedimentary Sequence in the Munger-Rajgir Metasedimentary Belt, Gaya District, Bihar. *Indian Journal of Geoscience* **63**, 351–60.

Ahmad M, Paul AQ, Negi P, Akhtar S, Gogoi B, and Saikia A (2021) Mafic rocks with back-arc E-MORB affinity from the Chotanagpur Granite Gneiss Complex of India: relicts of a Proterozoic Ophiolite suite. *Geological Magazine* **158**, 1527–42.

Ahmad T and Tarney J (1991) Geochemistry and petrogenesis of Garhwal volcanics: implications for evolution of the north Indian lithosphere. *Precambrian Research* **50**, 69–88.

Alam M, Choudhary AK, Mouri H and Ahmad T (2017) Geochemical characterization and petrogenesis of mafic granulites from the Central Indian Tectonic Zone (CITZ). *Geological Society, London, Special Publications* **449**, 207–29.

Anderson D (1995) Lithosphere, asthenosphere, and perisphere. *Reviews of Geophysics* **33**, 125–49.

Anderson JL (1996) Status of thermobarometry in granitic batholiths. *Transactions of Royal Society Edinburgh, Earth Sciences* **87**, 125–38.

https://doi.org/10.1017/S0016756823000237 Published online by Cambridge University Press

Anderson JL and Smith DR (1995) The effects of temperature and fO_2 on the Al-in hornblende barometer. *American Mineralogist* **8**, 549–59.

Awati AB, Harikrishnan T, Sinha RM, Gupta KR and Gupta RK (1995) The Proterozoic Shillong basin of North East India: conceptual model for hosting unconformity related uranium mineralization. *Exploration and Research for Atomic Minerals* **8**, 141–54.

Balaram V, Saxena VK, Manikyamba C and Ramesh SL (1990) Determination of rare earth elements in Japanese rock standards by inductively coupled plasma mass spectrometry. *Atomic Spectroscopy* **11**, 19–23.

Bhandari A, Pant NC, Bhowmik SK and Goswami S (2011) _1.6 Ga ultrahigh-temperature granulite metamorphism in the Central Indian Tectonic Zone: insights from metamorphic reaction history, geothermobarometry and monazite chemical ages. *Geological Journal* **46**, 198–216.

Bhattacharjee CC and Rahman S (1985) Structure and lithostratigraphy of the Shillong Group of rocks in East Khasi hills of Meghalaya. *Bulletin of Geological Mining and Metallurgy Society of India* **53**, 90–9.

Bhowmik SK (2019) The current status of orogenesis in the Central Indian Tectonic Zone: a view from its Southern Margin. *Geological Journal* **54**, 2912–34.

Bhowmik SK, Wilde SA and Bhandari A (2011) Zircon U–Pb/Lu–Hf and monazite chemical dating of the tirodi biotite gneiss: implication for Latest Paleoproterozoic to Early Mesoproterozoic Orogenesis in the Central Indian Tectonic Zone. *Geological Journal* **46**, 574–96.

Bhowmik SK, Wilde SA, Bhandari A, Pal T and Pant NC (2012) Growth of the Greater Indian landmass and its assembly in Rodinia: geochronological evidence from the Central Indian Tectonic Zone. *Gondwana Research* **22**, 54–72.

Bidyananda M and Deomurari MP (2007) Geochronological constraints on the evolution of Meghalaya massif, northeastern India: an ion microprobe study. *Current Science* **93**, 1620–3.

Blundy JD and Holland TJB (1990) Calcic amphibole equilibria and a new amphibole plagioclase geothermometer. *Contributions to Mineralogy and Petrology* **104**, 208–24.

Bora S, Kumar S, Yi K, Kim N and Lee TH (2013) Geochemistry and U-Pb SHRIMP zircon chronology of granitoids and microgranular enclaves from Jhirgadandi Pluton of Mahakoshal Belt, Central India Tectonic Zone, India. *Journal of Asian Earth Sciences* **70–71**, 99–114.

Boynton WV (1984) Cosmochemistry of the rare earth elements: meteorite studies. In Developments in geochemistry, *Elsevier* 2, 63–114.

Chatterjee N and Ghose NC (2011) Extensive Early Neoproterozoic high-grade metamorphism in North Chotanagpur Gneissic Complex of the Central Indian Tectonic Zone. *Gondwana Research* **20**, 362–79.

Chatterjee N, Bhattacharya A, Duarah BP and Mazumdar AC (2011) Late Cambrian reworking of Paleo-Mesoproterozoic granulites in Shillong-Meghalaya gneissic complex (Northeast India): evidence from PT pseudo-section analysis and monazite chronology and implications for East Gondwana assembly. *The Journal of Geology* **119**, 311–30.

Chatterjee N, Crowley JI and Ghose NC (2008) Geochronology of the 1.55 Ga Bengal anorthosite and Grenvillian metamorphism in the Chotanagpur Gneissic complex, eastern India. *Precambrian Research* **161**, 303–16.

Chatterjee N, Mazumdar AC, Bhattacharya A and Saikia RR (2007) Mesoproterozoic granulites of the Shillong-Meghalaya Plateau: evidence of westward continuation of the Prydz Bay Pan-African suture into Northeastern India. *Precambrian Research* **152**, 1–26.

Chattopadhyay A, Bhowmik SK and Roy A (2020) Tectonothermal evolution of the Central Indian Tectonic Zone and its implications for Proterozoic supercontinent assembly: the current status. *Episodes Journal of International Geoscience* **43**, 132–44.

Condie KC, Bobrow DJ and Card KD (1987) Geochemistry of Precambrian mafic dikes from the southern Superior Province. In *Mafic dike swarms* (eds HC Halls and WF Fahrig), pp. 95–108. *Geological Association of Canada Special Paper* 34.

Desikachar OSV (1974) A review of the tectonic and geological history of eastern India in terms of 'plate tectonics' theory. *Journal of the Geological Society of India* **33**, 137–49.

Dhurandhar AP, Pandey UK and Raminaidu C (2019) Petrochemistry and Sr, Nd, Pb isotopic characteristics of basic Dykes of Mikir Hills, Assam. *Journal of the Geological Society of India* **94**, 559–72.

Dobmeier C, Lütke S, Hammerschmidt K, and Mezger K (2006) Emplacement and deformation of the Vinukonda meta-granite (Eastern Ghats, India)—Implications for the geological evolution of peninsular India and for Rodinia reconstructions. *Precambrian Research* **146**, 165–178.

Doley D, Bhagabaty B, Sarma G, Singh AK and Zou X (2022) Geochemistry of Late Palaeoproterozoic (1.69 Ga) A-type Mayong granitoids in Shillong Plateau, north-east India: implication for anorogenic magmatism during Columbia Supercontinent cycle. *Geological Journal* **57**, 662–80.

Ermenco NA, Negi BS, Nasianov MV, Seregin AM, Despande BG, Sengupta SN, Talukdar SN, Sastri VV, Sokaluv IP, Pavbukov AT, Dutta AK and Raju ATR (1969) Tectonic map of India–Principles of preparation. *Bulletin of ONGC* **6**, 1–111.

Espanon VR, Chivas AR, Kinsley LPJ and Dosseto A (2014) Geochemical variations in the Quaternary Andean back-arc volcanism, southern Mendoza, Argentina. *Lithos* **208–209**, 251–64.

Evans DAD (2013) Reconstructing pre-Pangean supercontinents. *Geological Society of America Bulletin* **125**, 1735–51.

Finlow-Bates T and Stumpfl EF (1981) The behaviour of so-called immobile elements in hydrothermally altered rocks associated with volcanogenic submarine-exhalative ore deposits. *Mineralium Deposita* **16**, 319–28.

Fitton JG, James D, Kempton PD, Ormerod DS and Leeman WP (1988) The role of lithospheric mantle in the generation of late Cenozoic basic magmas in the western United States. *Journal of Petrology* **1**, 331–49.

Fleet ME and Barnett RL (1978) $^{iv}Al/^{vi}Al$ partitioning in calciferous amphiboles from the Frood Mine Sudbury, Ontario. *Canadian Mineralogist* **16**, 527–32.

Ghose NC and Chatterjee N (2008) Petrology, tectonic setting and source of dykes and related magmatic bodies in the Chotanagpur Gneissic Complex, Eastern India. *Indian Dykes: Geochemistry, Geophysics and Geochronology* (eds RK Srivastava, C Sivaji and NV Chalapathi Rao), pp. 471–493. New Delhi, India: Narosa Publ. House Pvt. Ltd.

Ghosh S, Bhalla JK, Paul DK, Sarkar A, Bishui PK and Gupta SN (1991) Geochronology and geochemistry of granite plutons from East Khasi Hills, Meghalaya. *Journal of the Geological Society of India* **37**, 331–42.

Ghosh S, Fallick AE, Paul DK and Potts PJ (2005) Geochemistry and origin of Neoproterozoic granitoids of Meghalaya, Northeast India: implications for linkage with amalgamation of Gondwana supercontinent. *Gondwana Research* **8**, 421–32.

Gogoi A, Majumdar D, Cottle J and Dutta P (2019) Geochronology and geochemistry of Mesoproterozoic porphyry granitoids in the northern Karbi Hills, NE India: implications for early tectonic evolution of the Karbi Massif. *Journal of Asian Earth Sciences* **79**, 65–79.

Gogoi B (2022) Late Paleoproterozoic bimodal magmatic rocks in the Nimchak Granite Pluton of the Bathani volcano-sedimentary sequence, Eastern India: implications for the Columbia supercontinent formation with respect to the Indian landmass. *Periodico di Mineralogia* **91**, 1–20.

Gorton MP and Schandl ES (2000) From continents to island arcs: a geochemical index of tectonic setting for arc-related and within-plate felsic to intermediate volcanic rocks. *Canadian Mineralogist* **38**, 1065–73.

Grove T, Parman S, Bowring S, Price R and Baker M (2002) The role of an H_2O-rich fluid component in the generation of primitive basaltic andesites and andesites from the Mt. Shasta region, N California. *Contributions to Mineralogy and Petrology* **142**, 375–96.

Guo F, Li H, Fan W, Li J, Zhao L, Huang M and Xu WL (2015) Early Jurassic subduction of the Paleo-Pacific Ocean in NE. China: petrologic and geochemical evidence from the Tumen mafic intrusive complex. *Lithos* **224**, 40–60.

Hawkesworth CJ, Gallagher K, Hergt JM and McDermott F (1993) Mantle slab contributions in arc magmas. *Annual Review of Earth and Planetary Sciences* **21**, 175–204.

Hawkesworth CJ, Turner SP, McDermott F, Peate DW and Van Calsteren P (1997) U-Th isotopes in arc magmas: implications for element transfer from the subducted crust. *Science* **276**, 551–5.

Hawthorne FC, Oberti R, Harlow GE, Maresch WV, Martin RF, Schumacher JC and Welch MD (2012) Nomenclature of the amphibole group. *American Mineralogist* **97**, 2031–48.

Hazra S and Ray J (2009) Nature of mafic magmatism in 'Khasi Greenstone' around Laitlyngkot, East Khasi Hills, Meghalaya, northeastern India. *Indian Journal of Geology* **79**, 47–58.

Holland TJB and Blundy JD (1994) Non-ideal interactions in calcic amphiboles and their bearing on amphibole–plagioclase thermometry. *Contributions to Mineralogy and Petrology* **116**, 433–47.

Hollister LS, Grissom GC, Peters EK, Stowell HH and Sisson VB (1987) Confirmation of the empirical correlation of Al in hornblende with pressure of solidification of calc-alkaline plutons. *American Mineralogist* **72**, 231–9.

Hossain I, Tsunogae T, Rajesh HM, Chen B and Arakawa Y (2007) Palaeoproterozoic U–Pb SHRIMP zircon age from basement rocks in Bangladesh: a possible remnant of the Columbia Supercontinent. *Comptes Rendus Geoscience* **339**, 979–86.

Hou G, Santosh M, Qian X, Lister GS and Li J (2008) Configuration of the Late Paleoproterozoic super continent Columbia: insights from radiating mafic dyke swarms. *Gondwana Research* **14**, 395–409.

Irvine TN and Baragar WRA (1971) A guide to the geochemical classification of the common volcanic rocks. *Canadian Journal of Earth Sciences* **8**, 523–48.

Kaur P, Zeh A, Chaudhri N, Gerdes A and Okrusch M (2013) Nature of magmatism and sedimentation at a Columbia active margin: insights from combined U–Pb and Lu–Hf isotope data of detrital zircons from NW India. *Gondwana Research* **23**, 1040–52.

Kumar A and Ahmad T (2007) Geochemistry of mafic dykes in part of Chotanagpur gneissic complex: petrogenetic and tectonic implications. *Geochemical Journal* **41**, 173–86.

Kumar S (1990) Petrochemistry and geochronology of pink granite from Sonsak, East Garo Hills, Meghalaya. *Journal of Geological Society of India* **35**, 39–45.

Kumar S, Rino V, Hayasaka Y, Kimura K, Raju S, Terada K, and Pathak M (2017) Contribution of Columbia and Gondwana Supercontinent assembly- and growth-related magmatism in the evolution of the Meghalaya Plateau and the Mikir Hills, Northeast India: constraints from U-Pb SHRIMP zircon geochronology and geochemistry. *Lithos* **277**, 356–75.

Le Bas MJ, Le Maitre RW, Streckeisen A and Zanettin B (1986) A chemical classification of volcanic rocks based on the total alkalies-silica diagram. *Journal of Petrology* **27**, 745–50.

Liu B, Ma CQ, Zhang JY, Xiong FH, Huang J and Jiang HA (2014) 40Ar–39Ar age and geochemistry of subduction-related mafic dikes in northern Tibet, China: petrogenesis and tectonic implications. *International Geology Review* **56**, 57–73.

MacLean WH and Barrett TJ (1993) Lithogeochemical techniques using immobile elements. *Journal of Geochemical Exploration* **48**, 109–33.

Majumdar D and Gogoi A (2020) Prospectivity of Mesoproterozoic magmatism in the northern Karbi Hills, NE India for porphyry copper mineralization. *Ore Geology Reviews* **120**, 103467.

Mallikharjuna Rao J, Poornachandra Rao GVS and Sarma KP (2009) Precambrian mafic magmatism of Shillong Plateau, Meghalaya and their evolutionary history. *Journal of the Geological Society of India* **73**, 143–52.

Mazumder SK (1986) The Precambrian framework of the Khasi Hills, Meghalaya. *Record Geological Survey of India* **117**, 1–59.

McKenzie D and O'Nions RK (1991) Partial melt distributions from inversion of rare earth element. *Journal of Petrology* **32**, 1021–91.

Meert JG and Santosh M (2022) The Columbia supercontinent: retrospective, status, and a statistical assessment of paleomagnetic poles used in reconstructions. *Gondwana Research* **110**, 143–64.

Menzies MA, Kyle PR, Jones M and Ingram G (1991) Enriched and depleted source components for tholeiitic and alkaline lavas from Zuni-Bandera, New Mexico: inferences about intraplate processes and stratified lithosphere. *Journal of Geophysical Research: Solid Earth* **96**, 13645–71.

Miyashiro A (1973) Paired and unpaired metamorphic belts. *Tectonophysics* **17**, 241–54.

Miyashiro A (1994) *Metamorphic Petrology*. Boca Raton, FL: CRC Press.

Mohr PA (1987) Crustal contamination in mafic sheets: a summary. In *Mafic Dyke Swarms* (eds HC Halls and WC Fahrig), pp. 75–80. St John's: Geological Association of Canada, Special Publication no. 34.

Nachit H, Ibhi A and Ohoud MB (2005) Discrimination between primary magmatic biotites, reequilibrated biotites and neoformed biotites. *Comptes Rendus Geoscience* **337**, 1415–20.

Nandy DR (2001) Geodynamics of northeastern India and the adjoining region. *ACB Publications*, 111–130.

Ormerod DS, Hawkesworth CJ, Leeman WP and Menzies MA (1988) The identification of subduction-related and within-plate components in basalts from the western U.S.A. *Nature* **333**, 349–53.

Pandey BK, Gupta JN and Lall Y (1986) Whole-rock and mineral Rb–Sr isochron ages for the granites of Bihar Mica Belt of Hazaribagh, Bihar, India. *Indian Journal of Earth Sciences* **13**, 157–62.

Peacock SM, Rushmer T and Thompson AB (1994) Partial melting of subducting oceanic crust. *Earth and planetary science letters* **121**, 227–44.

Pearce JA (1996) A users guide to basalt discrimination diagrams. In *Trace Element Geochemistry of Volcanic Rocks: Applications for Massive Sulphide Exploration* (ed. DA Wyman), pp. 79–113. St. John's, Canada: Geological Association of Canada, Short Course Notes no. 12.

Pearce JA (2008) Geochemical fingerprinting of oceanic basalts with applications to the ophiolites classification and the search for Archean oceanic crust. *Lithos* **100**, 14–48.

Pearce JA and Cann JR (1973) Tectonic setting of basic volcanic rocks determined using trace element analyses. *Earth and Planetary Science Letters* **19**, 290–300.

Pearce JA and Norry MJ (1979) Petrogenetic implications of Ti, Zr, Y, and Nb variations in volcanic rocks. *Contributions to Mineralogy and Petrology* **69**, 33–47.

Pearce JA and Peate DW (1995) Tectonic implications of the composition of volcanic arc magmas. *Annual Review of Earth and Planetary Sciences* **23**, 281–5.

Pearce JA and Stern RJ (2006) Origin of back-arc basin magmas: trace element and isotope perspectives. In *Back-Arc Spreading Systems; Geological, Biological, Chemical, and Physical Interactions* (eds DM Christie, CR Fisher, SM Lee and S Givens), pp. 63–86. *Geophysical Monograph Series* 166. Washington, DC: American Geophysical Union.

Pe-piper G, Matarangas D, Reynolds PH and Chatterjee AK (2003) Shoshonites from Agios Nectarios, Lesbos, Greece: origin by mixing of felsic and mafic magma. *European Journal of Mineralogy* **15**, 77–8.

Pesonen LJ, Mertanen S and Veikkolainen T (2012) Paleo-Mesoproterozoic supercontinents – a paleomagnetic view. *Geophysica* **48**, 5–47.

Pisarevsky SA, Biswal TK, Wang XC, DeWaele B, Ernst R, Södurlund U, Tait JA, Ratre K, Singh YK and Cleve M (2013) Palaeomagnetic, geochronological and geochemical study of Mesoproterozoic Lakhna Dykes in the Bastar Craton, India: implications for the Mesoproterozoic supercontinent. *Lithos* **174**, 125–43.

Pouchou JL and Pichoir F (1987) Basic expression of "PAP" computation for quantitative EPMA. In *X-ray Optics and Microanalysis* (eds JD Brown and RH Packwood), pp. 249–253. Ontario: University of Western Ontario.

Ray Barman T and Bishui PK (1994) Dating of Chotanagpur gneissic complex of eastern Indian Precambrian shield. *Record Geological Survey of India* **127**, 25–27.

Ray Barman T, Bishui PK and Sarkar A (1990) Dating of Early Precambrian Granite-Greenstone Complex of the eastern Indian Precambrian shield with special references to Chotanagpur Granite Gneiss Complex. *Records of the Geological Survey of India* **123**, 25–7.

Ray J, Saha A, Koeberl C, Thoni M, Ganguly S and Hazra S (2013) Geochemistry and petrogenesis of Proterozoic mafic rocks from East Khasi Hills, Shillong Plateau, Northeastern India. *Precambrian Research* **230**, 119–37.

Redman BA and Keays RR (1985) Archaean basic volcanism in the Eastern Goldfields Province, Yilgarn Block, Western Australia. *Precambrian Research* **30**, 113–52.

Rekha S, Upadhyay D, Bhattacharya A, Kooijman E, Goon S, Mahato S and Pant NC (2011) Lithostructural and chronological constraints for tectonic restoration of Proterozoic accretion in the Eastern Indian Precambrian shield. *Precambrian Research* **187**, 313–33.

Rollinson HR (1993) *Using Geochemical Data: Evaluation, Presentation, Interpretation*. New Jersey: Pearson Prentice Hall, 352.

https://doi.org/10.1017/S0016756823000237 Published online by Cambridge University Press

Saha D, Bhowmik SK, Bose S and Sajeev K (2016) Proterozoic tectonics and trans-Indian mobile belts: a status report. *Proceedings of the Indian National Science Academy* **82**, 445–60.

Saikia A, Gogoi B, Ahmad M, Kumar R, Kaulina T and Bayanova T (2019) *Mineral chemistry, Sr-Nd isotope geochemistry and petrogenesis of the granites of Bathani volcano-sedimentary sequence from the northern fringe of Chotanagpur Granite Gneiss Complex of eastern India*. Bern: Springer Nature, Society of Earth Scientists, pp. 79–120.

Saikia A, Gogoi B, Kaulina T, Lialina L, Bayanova T and Ahmad M (2017) Geochemical and U–Pb zircon age characterization of granites of the Bathani volcano-sedimentary sequence, Chotanagpur granite gneiss complex, Eastern India: vestiges of the Nuna supercontinent in the Central Indian Tectonic Zone. In Crustal Evolution of India and Antarctica: The Supercontinent Connection. *Geological Society of London, Special Publication* 457, 233–252.

Saini NK, Mukherjee PK, Rathi MS and Khanna PP (2000) Evaluation of energy-dispersive x-ray fluorescence spectrometry in the rapid analysis of silicate rocks using pressed powder pellets. *X-Ray Spectrometry* **29**, 166–72.

Saini NK, Mukherjee PK, Rathi MS, Khanna PP and Purohit KK (2007) A proposed amphibolite reference rock sample (AMH) from Himachal Pradesh. *Journal of Geological Society of India* **69**, 799–802.

Sarkar A, Boda MS, Kundu HK, Mamgain VV and Shankar R (1998) Geochronology and geochemistry of Mesoproterozoic intrusive plutonites from the eastern segment of the Mahakoshal greenstone belt, Central India. In: International Seminar on Precambrian Crust in Eastern and Central India, UNESCOIUGS- IGCP-368, Abstract Volume. Geological Survey of India, Kolkata, 82–85.

Saunders AD, Tarney J and Weaver SD (1980) Transverse geochemical variations across the Antarctic Peninsula: implications for the genesis of calc-alkaline magmas. *Earth and Planetary Science Letters* **46**, 344–60.

Schmidt MW (1992) Amphibole composition in tonalite as a function of pressure: an experimental calibration of the Al-in-hornblende barometer. *Contributions to Mineralogy and Petrology* **110**, 304–10.

Sequeira N, Bhattacharya A and Bell E (2022) The~ 1.4 Ga A-type granitoids in the "Chottanagpur crustal block"(India), and its relocation from Columbia to Rodinia? *Geoscience Frontiers* **13**, 101138.

Sheraton JW, Black LP, McCulloch MT and Oliver RL (1990) Age and origin of a compositionally varied mafic dyke swarm in the Bunger Hills, East Antarctica. *Chemical Geology* **85**, 215–46.

Smith EI, Sánchez A, Walker JD and Wang K (1999) Geochemistry of mafic magmas in the Hurricane volcanic field, Utah: implications for small- and large-scale chemical variability of the lithospheric mantle. *The Journal of Geology* **107**, 433–48.

Spandler C and Pirard C (2013) Element recycling from subducting slabs to arc crust: a review. *Lithos* **170–171**, 208–23.

Srinivasan P, Sen S and Bandopadhyay PC (1996) Study of variation of Palaeocene Eocene sediments in the shield areas of Shillong Plateau. *Records of Geological Survey of India* **129**, 77–8.

Srivastava RK (2012) Petrological and geochemical studies of paleoproterozoic mafic dykes from the Chitrangi Region, Mahakoshal Supracrustal Belt, Central Indian Tectonic Zone: petrogenetic and tectonic significance. *Journal of the Geological Society of India* **80**, 369–81.

Srivastava RK and Ahmad T (2008) Precambrian mafic magmatism in the Indian shield: an introduction. *Journal of the Geological Society of India* **72**, 9–14.

Srivastava RK and Sinha AK (2004) Geochemistry and Petrogenesis of early Cretaceous sub alkaline mafic dykes from Swangkre–Rongmil, East Garo Hills, Shillong Plateau, NE India. *Journal of Earth System Science* **113**, 683–97.

Stern CR and Kilian R (1996) Role of the subducted slab, mantle wedge and continental crust in the generation of adakites from the Andean Austral Volcanic Zone. *Contributions to Mineralogy and Petrology* **123**, 263–81.

Stolper E and Newman S (1994) The role of water in the petrogenesis of Mariana trough magmas. *Earth and Planetary Science Letters* **121**, 293–325.

Su YP, Zheng JP, Griffin WL, Zhao JH, Tang HY, Ma Q and Lin XY (2012) Geochemistry and geochronology of Carboniferous volcanic rocks in the eastern Junggar terrane, NW China: implication for a tectonic transition. *Gondwana Research* **22**, 1009–29.

Sun SS and McDonough WF (1989) Chemical and isotopic systematics of oceanic basalts: implications for mantle composition and processes. *Geological Society, London, Special Publications* **42**, 313–45.

Thomas WM and Ernst WG (1990) The aluminum content of hornblende in calc-alkaline granitic rocks: a mineralogic barometer calibrated experimentally to 12 kbars. In *Fluid–mineral interactions: a tribute to HP Eugster* (eds RJ Spencer and IM Chou), pp. 59–63. *Geochemical society of London Special Publication* 2.

Thompson RN and Morrison MA (1998) Asthenospheric and lower-lithospheric mantle contributions to continental extensional magmatism: an example from the British Tertiary Province. *Chemical Geology* **68**, 1–15.

Tischendorf G, Gottesmann B, Förster HJ and Trumbull RB (1997) On Li-bearing micas: estimating Li from electron microprobe analyses and improved diagram for graphical representation. *Mineralogical Magazine* **61**, 809–34.

Turner S, Hawkesworth C, Rogers N and King P (1997) U-Th isotope disequilibria and ocean island basalt generation in the Azores. *Chemical Geology* **139**, 145–64.

Wang C, He X, Carranza EJM and Cui C (2019) Paleoproterozoic volcanic rocks in the southern margin of the North China Craton, central China: implications for the Columbia supercontinent. *Geoscience Frontiers* **10**, 1543–60.

Watts AB and Cox KG (1989) The Deccan Traps: an interpretation on terms of progressive lithospheric flexure in response to a migrating lead. *Earth and Planetary Science Letters* **93**, 85–97.

Wilson M and Davidson JP (1984) The relative roles of crust and upper mantle in the generation of oceanic island-arc magmas. *Philosophical Transactions of Royal Society of London A* **310**, 661–74.

Woodhead J, Eggins S and Gamble J (1993) High-field strength and transition element systematics in island arc and back-arc basin basalts: evidence for multiphase melt extraction and a depleted mantle wedge. *Earth and Planetary Science Letters* **114**, 491–504.

Wyllie PJ (1988) Magma genesis, plate tectonics, and chemical differentiation of the Earth. *Reviews of Geophysics* **26**, 370–404.

Yadav B, Ahmad T, Kaulina T and Bayanova T (2015) Geochemistry and petrogenesis of Paleo-Proterozoic granitoids from Mahakoshal Supracrustal Belt (MSB), CITZ. *EGU General Assembly Conference Abstracts* **17**, 5256.

Yin A, Dubey CS, Webb AAG, Kelty TK, Grove M, Gehrels GE and Burgess WP (2010) Geologic correlation of the Himalayan orogen and Indian craton: part 1. Structural geology, U-Pb zircon geochronology, and tectonic evolution of the Shillong Plateau and its neighboring regions in NE India. *GSA Bulletin* **122**, 336–59.

Zhang S, Li ZX, Evans DAD, Wu H, Li H and Dong J (2012) Pre-Rodinia supercontinent Nuna shaping up: a global synthesis with new paleomagnetic results from North China. *Earth and Planetary Science Letters* **353–354**, 145–55.

Zhao G, Cawood PA, Wilde SA and Sun M (2002) Review of global 2.1-1.8 Ga orogens: implications for a pre-Rodinia supercontinent. *Earth-Science Reviews* **59**, 125–62.

Zhao JX, Shiraishi K, Ellis DJ and Sheraton JW (1995) Geochemical and isotopic studies of syenites from the Yamato Mountains, East Antarctica: implications for the origin of syenitic magmas. *Geochimica et Cosmochimica Acta* **59**, 1363–82.

https://doi.org/10.1017/S0016756823000237 Published online by Cambridge University Press